

Spatial variation of the crustal stress field along the Ryukyu-Taiwan-Luzon convergent boundary

Wen-Nan Wu,^{1,2} Honn Kao,³ Shu-Kun Hsu,¹ Chung-Liang Lo,^{1,2} and How-Wei Chen¹

Received 27 October 2009; revised 17 June 2010; accepted 28 July 2010; published 5 November 2010.

[1] We applied an improved stress inversion method to a comprehensive data set of earthquake focal mechanisms to depict the pattern of crustal stress along the western convergent boundary of the Philippine Sea plate. Our results indicate that the crustal stress along the Ryukyu fore arc is segmented with boundaries at or near the places of seamount subduction, including the Tokara channel. An extensional stress regime is observed along the entire Ryukyu back arc, implying that back-arc rifting may have extended northward to Kyushu. A triangular area near the southernmost terminus of the Ryukyu arc is characterized by a unique stress signature. The eastern boundary of this Ryukyu-Taiwan Stress Transition coincides with the 123°E meridian where the Gagua ridge intercepts the Ryukyu trench; whereas its western boundary agrees remarkably well with the border between the postcollision and waning-collision domains in northern Taiwan. The Taiwan collision zone is dominated by compression that rotates locally according to the structural configuration of the Lukang Magnetization High (LMH), suggesting that the LMH may be critical in controlling the local stress distribution. The stress signature of the Luzon arc-Taiwan collision reaches as far south as 19.5°N. The tectonic stress along the Manila trench-Luzon fore arc is dominated by a complex regime of extension that cannot be explained by simple plate bending or in-slab membrane stress. Since this extensional regime is observed only south of ~22°N, it probably marks the northern limit of the contemporary boundary between the subduction along the Manila trench and the collision in Taiwan.

Citation: Wu, W.-N., H. Kao, S.-K. Hsu, C.-L. Lo, and H.-W. Chen (2010), Spatial variation of the crustal stress field along the Ryukyu-Taiwan-Luzon convergent boundary, *J. Geophys. Res.*, 115, B11401, doi:10.1029/2009JB007080.

1. Introduction

[2] The Ryukyu-Taiwan-Luzon boundary marks the western side of the Philippine Sea plate (PSP) where the regional tectonics is dominated by the convergent processes with respect to the Eurasia plate (EP) (Figure 1). To the north of Taiwan, the relative plate motion is accommodated by the subduction of PSP beneath the Ryukyu arc; whereas to the south the PSP overrides the EP along the Manila trench [e.g., Biq, 1972; Suppe, 1984; Tsai et al., 1977; Wu, 1978]. In between, the northwestward indentation of the Luzon arc results in the Taiwan orogenic belt [e.g., Angelier et al., 1986; Suppe, 1984], characterized by active tectonic deformation with frequent seismicity (Figures 1 and 2).

[3] To fully understand the seismotectonic patterns in the Ryukyu-Taiwan-Luzon margin, one of the fundamental

steps is to systematically examine the spatial variation of the tectonic stress regime across the entire region. To some extent, it has been partially investigated by many previous studies on the basis of earthquake focal mechanisms along the Ryukyu arc [e.g., Kao and Chen, 1991; Kao et al., 1998a, 1998b; Shiono et al., 1980], the northern Luzon arc [e.g., Bautista et al., 2001; Galgana et al., 2007; Kao et al., 2000], and in the Taiwan collision zone [e.g., Chang et al., 2003; Hsu et al., 2009; Kao et al., 1998b; Kao and Jian, 2001; Pezzopane and Wesnousky, 1989; Rau et al., 1996; Rau and Wu, 1998; Wu et al., 2008]. However, using the distribution of compressional (P -) and extensional (T -) axes of earthquake focal mechanisms as a proxy to the principal axes of regional tectonic stress is known to have significant limitations, especially in regions where the number of fault plane solutions is scarce and/or the occurrence of earthquakes is dominated by the orientations of preexisting zones of weakness [e.g., Gephart and Forsyth, 1984; McKenzie, 1969].

[4] There were also studies to invert the tectonic stress regimes directly from earthquake focal mechanisms for the Ryukyu arc [e.g., Christova, 2004; Kubo and Fukuyama, 2003], the northern Luzon arc [e.g., W.-N. Wu et al., 2009], and the Taiwan collision zone [e.g., Hsu et al., 2009; Kao and Angelier, 2001; Rau and Wu, 1998; Wu et al., 2008; Yeh et al.,

¹Institute of Geophysics, National Central University, Chung-Li, Taiwan.

²Now at Institute of Earth Sciences, Academia Sinica, Taipei, Taiwan.

³Geological Survey of Canada, Pacific Geoscience Centre, Sidney, British Columbia, Canada.

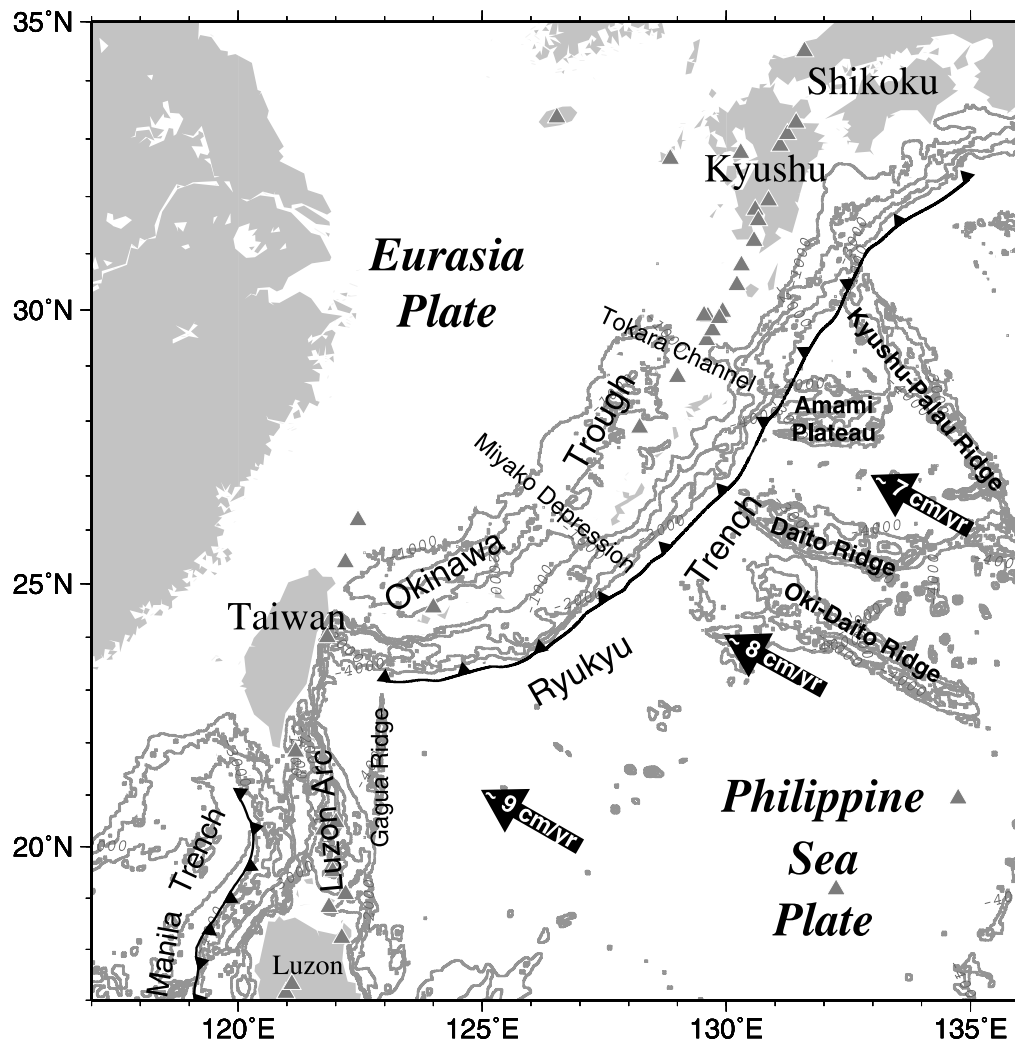


Figure 1. Map showing the tectonic setting of the study area. The Taiwan orogenic belt is located in the middle of the western margin of the Philippine Sea plate, with the Ryukyu and Luzon subduction systems to the northeast and south, respectively. The relative plate motion between the Philippine Sea and Eurasia plates is calculated from the HS3-NUVEL-1A model [Gripp and Gordon, 2002] and shown by arrows. Triangles mark the locations of volcanoes.

1991]. Although the stress inversion method has been constantly improved over the past two decades [e.g., Abers and Gephart, 2001; Angelier, 1984; Arnold and Townsend, 2007; Gephart and Forsyth, 1984; Gephart, 1990; Hardebeck and Michael, 2006; Michael, 1984, 1987; Terakawa and Matsu'ura, 2008; Yin and Ranalli, 1993], two issues remain to be the major concerns in the inversion process. First of all, the inversion is well constrained only if a diverse pattern of earthquake focal mechanisms is available. In other words, uncertainties in the principal stress orientations can be large when nearly all earthquakes appear to have the same mechanism. Second, all stress inversion methods assume that the observed diverse pattern of earthquake focal mechanisms is associated with a uniform stress field. When a region is characterized by a complex tectonic environment consisting of several different stress regimes, it becomes necessary to set up subregions so that the assumption of a uniform stress field

is not violated. Under such a scenario, the inversion result can depend on how the study area is partitioned [Hardebeck and Michael, 2006; Terakawa and Matsu'ura, 2008].

[5] Furthermore, most previous works addressed limited portions of the convergent margin along the west side of the PSP, primarily due to the geographic coverage of their data sets. In this study, we attempt to delineate the detailed crustal stress pattern of the western PSP boundary along the entire Ryukyu-Taiwan-Luzon convergent zone by compiling a joint data set from both global and regional seismic catalogs. The stress inversion method recently developed by Hardebeck and Michael [2006] is used to avoid the possible bias due to the subjective choice of area partition scheme. Our results not only present a more complete picture on the state of crustal stress along the convergent boundary of the west PSP, but also demonstrate in an unprecedented resolution how the tectonic stress varies spatially from one

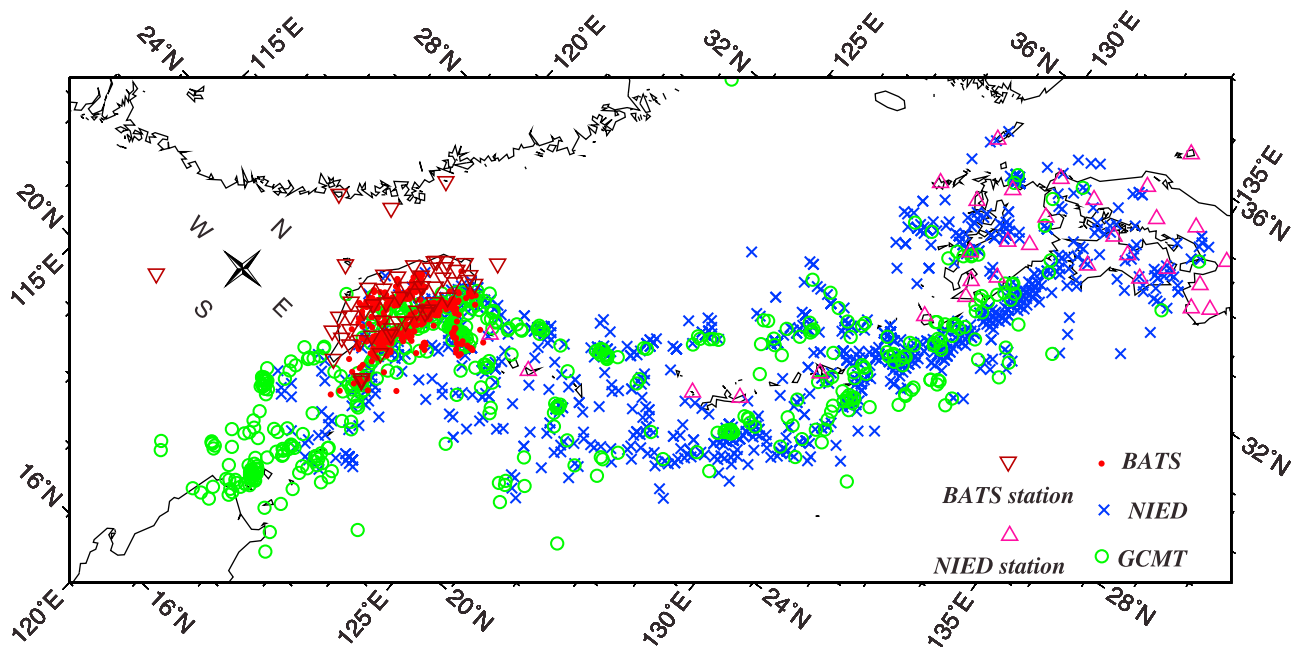


Figure 2. Epicentral distribution of crustal earthquakes (depth ≤ 35 km) used in this study. Different symbols represent events whose focal mechanisms are reported by different groups. In addition to solutions from the Global CMT Project (GCMT), the completeness of our data set is significantly improved by including reliable earthquake focal mechanisms from the two regional broadband seismograph networks, BATS and NIED, shown by inverted triangles and triangles, respectively.

regime to another in connection with the regional tectonic processes and structures. Finally, the interaction among different tectonic components in terms of the orientations of principal stress axes is discussed.

2. Data and Analysis

2.1. Earthquake Focal Mechanisms

[6] The Harvard centroid moment tensor (CMT) [Dziewonski *et al.*, 1981] catalog has been thoroughly examined and is generally accepted as the best earthquake source parameter data set for its completeness and accuracy [Kagan, 2003]. Since the summer of 2006, the Harvard CMT Project has migrated into a new phase named as “The Global CMT Project” (GCMT) (<http://www.globalcmt.org>). Despite its merits, the GCMT catalog covers only large and moderate-sized events capable of generating sufficient signals at teleseismic distances. For the purpose of this study, however, inclusion of high-quality focal mechanism data for smaller earthquakes is apparently necessary.

[7] With the increasing knowledge of detailed regional velocity structures, the establishment of regional broadband networks, and the advance of applying CMT inversion technique to regional broadband waveforms, reliable earthquake source parameters for the Ryukyu-Taiwan-Luzon region can be obtained for events as small as $M_w \sim 3.5$ [e.g., Kao *et al.*, 1998a; Kubo *et al.*, 2002]. In this study, two regional CMT catalogs are included in addition to the GCMT. The first one is compiled by the Institute of Earth Sciences, Academia Sinica, based on the digital records of the Broadband Array in Taiwan for Seismology (BATS) (<http://bats.earth.sinica.edu.tw>) [e.g., Kao *et al.*, 1998a; Kao

and Jian, 2001]. The second one is reported by the National Research Institute for Earth Science and Disaster Prevention of Japan (NIED) (<http://www.hinet.bosai.go.jp/fnet>) using waveforms from the Full Range Seismograph Network of Japan [e.g., Kubo *et al.*, 2002]. The time span varies for each catalog depending on its operation history. The GCMT catalog is the longest, covering over 3 decades since January 1977. The BATS and NIED CMT catalogs are much shorter, starting in July 1995 and January 1997, respectively. The end date of our data set is 30 June 2008.

[8] Since the focus of this study is to resolve the crustal stress field, earthquakes deeper than 35 km are excluded to prevent contamination from the stress field within the subducted slab [e.g., Kao and Chen, 1991]. Moreover, we use a two-stage procedure in selecting events with better quality to minimize the effect of data uncertainties on the stress inversion results. Based on our best knowledge, there has been no quantitative study to systematically evaluate the accuracy of moment tensor solution catalogs for BATS or NIED. Therefore, the threshold of selecting CMT solutions from these two catalogs is determined empirically. For the BATS catalog, most of the CMT solutions with misfit ≤ 0.5 show good agreement between synthetic and observed seismograms. We provide three BATS inversion examples in Figure S1 in Text S1 to show that even inversion results with misfit between 0.5 and 0.6 are still of good quality.¹ Therefore, the threshold value of misfit ≤ 0.5 used in our study is appropriate. For the NIED CMT catalog, our

¹Auxiliary materials are available in the HTML. doi:10.1029/2009JB007080.

threshold (i.e., variation reduction $\geq 50\%$) is adopted directly from of NIED's official website (<http://www.fnet.bosai.go.jp/fnet/event/dreger.php?LANG=en>). In addition, to make sure that the inversion of CMT solution is robust, we only select events whose solution is determined with at least three stations. On the basis of the above selection criteria, we believe that all the used events have high quality and can reduce the effect of CMT error on the stress inversion. Statistical analysis of the GCMT catalog have indicated the average uncertainty of principal axes of earthquake moment tensors to be $\sim 15^\circ$ [e.g., *Frohlich and Davis*, 1999; *Frohlich*, 2001; *Helffrich*, 1997], too small to cause any significant rotation during stress tensor inversion [e.g., *Christova*, 2004; *Hardebeck and Hauksson*, 2001]. Therefore, we include all solutions from the GCMT catalog. In total, 2438 earthquake focal mechanisms are selected and their epicenters are marked in Figure 2.

[9] In the second stage, each focal mechanism is carefully checked to eliminate duplicates resulted from two or more catalogs reporting the same event. When duplicates are found, the final selection depends on the corresponding station distribution and signal-to-noise ratios of waveforms used in the CMT inversion. For the Ryukyu region (121°E – 135°E , 23°N – 35°N), the order of choice is usually NIED, BATS, then GCMT solutions. For Taiwan and its vicinity (119°E – 123.5°E , 21°N – 26°N), the order is BATS, GCMT, then NIED. For the northern Luzon region (119°E – 123°E , 18°N – 23.5°N), our first choice is the GCMT catalog because both regional networks provide poor station coverage. The final data set for our stress inversion contains 2296 earthquake focal mechanisms.

2.2. Data Processing and Damped Stress Inversion

[10] *Hardebeck and Michael* [2006] proposed an improved method for stress inversion from earthquake focal mechanisms. The inversion simultaneously minimizes the misfit between the stress tensor and focal mechanisms within each subarea and the difference between inverted stress tensors of adjacent subareas. The first objective is achieved using an algorithm similar to *Michael* [1984], while the second is accomplished by adding a least squares damping factor in the inversion process. The two biggest advantages of this method are (1) it can remove stress rotation artifacts that are resulted from arbitrary/subjective partition of the study area in an undamped inversion [*Hardebeck and Michael*, 2006], and (2) it can resolve a sharper pattern of true stress rotations than most other methods utilizing simple smoothing schemes (e.g., moving-window average).

[11] The procedure to perform a damped stress inversion is as following. First, we grid the study area based on the spatial distribution of events (Figure 2). The grid interval is 0.25° for the Taiwan region and 0.5° for the Ryukyu and Luzon regions (Figures 3a, 3d and 3g). We then simultaneously invert the reduced stress tensors for all grid nodes. For each node, the inversion requires a minimum of eight earthquakes located within the immediate vicinity (i.e., one grid interval). The number of earthquakes used to perform the stress inversion for each grid node is shown in Figures 3b, 3e and 3h.

[12] We calculate the average focal depth of events used for each grid node and compare it to the geometry of subducted slab based on the global slab model of *Syracuse and Abers* [2006] (Figures 3c, 3f and 3i). The results indicate

that most of the events used in our inversion are shallower than the plate interface, implying that the inverted stress field primarily corresponds to the overriding crust. Besides, *Kao and Chen* [1991] have demonstrated that the interplate thrust zone along most of the Ryukyu arc is aseismic down to a depth of ~ 30 km. Thus, the chance of our stress inversion being contaminated by events associated with the stress regime within the downgoing slab is minimal. It may be inevitable to have a few interplate earthquakes in our data set. We do not attempt to exclude interplate events because they could provide constraints on the forces that participate in the subduction geodynamics [*Christova*, 2004].

[13] The stress inversion practically minimizes the weighted sum of two values: the model length and the data variance [*Hardebeck and Michael*, 2006]. The model length is defined as the L2 norm of the vector containing the differences between each stress tensor component for each pair of adjacent grid nodes. The data variance is denoted by the L2 norm of the vector containing the differences between the data and the predictions of the model. The level of trade-off between these two quantities depends critically on the choice of the damping parameter, and we have performed a series of experiments to identify the optimal range, as shown in Figure 4. We choose a damping parameter of 1.0, 1.2, and 1.2 for the Taiwan, Ryukyu, and Luzon regions, respectively.

[14] For each grid node, the inversion result includes the azimuths and plunges of the principal stress axes (σ_1 , σ_2 , and σ_3), the ratio of stress differences, $\Phi = (\sigma_2 - \sigma_3)/(\sigma_1 - \sigma_3)$, and the 95% confidence interval of the stress orientations. The uncertainty in the orientation of the principal stress axes is estimated by bootstrap resampling of the entire data set for 2000 times. The boundary containing 95% of the bootstrap solutions closest to the preferred solution, as measured by the tensor dot product, is set to be the corresponding uncertainty [*Hardebeck and Michael*, 2006].

[15] It is well known that the focal mechanism data set used in stress inversion must be sufficiently diverse to provide adequate constraint on the orientation of the inverted principle stress axes [e.g., *Hardebeck and Hauksson*, 2001; *Hardebeck and Michael*, 2006; *Michael*, 1991]. To determine the mechanism diversity of each node, we compute the average focal mechanism followed by estimating its root-mean-square (RMS) angular differences with respect to individual fault plane solutions [*Kagan*, 2007; *Hardebeck and Hauksson*, 2001]. The diversity is deemed insufficient if the averaged angular difference is $\leq 45^\circ$. Such a threshold is determined from the uncertainties of earthquake source parameters of our data set and the results of inversion experiments reported in previous studies [e.g., *Hardebeck and Hauksson*, 2001]. Consequently, grid nodes falling below this threshold are marked with green crosses in Figure 5 to signal the likelihood of inadequate data constraint. These grid nodes are not used for further analysis.

[16] On the other hand, an extremely diverse data set might indicate that earthquakes used in the stress inversion are in fact associated with more than one stress regime. Theoretically if an equal number of focal mechanisms from two completely opposite stress regimes are mixed (e.g., pure thrust versus pure normal), the averaged angular difference (with respect to the average focal mechanism) should be 90° . To quantitatively assess that the stress inversion result for a

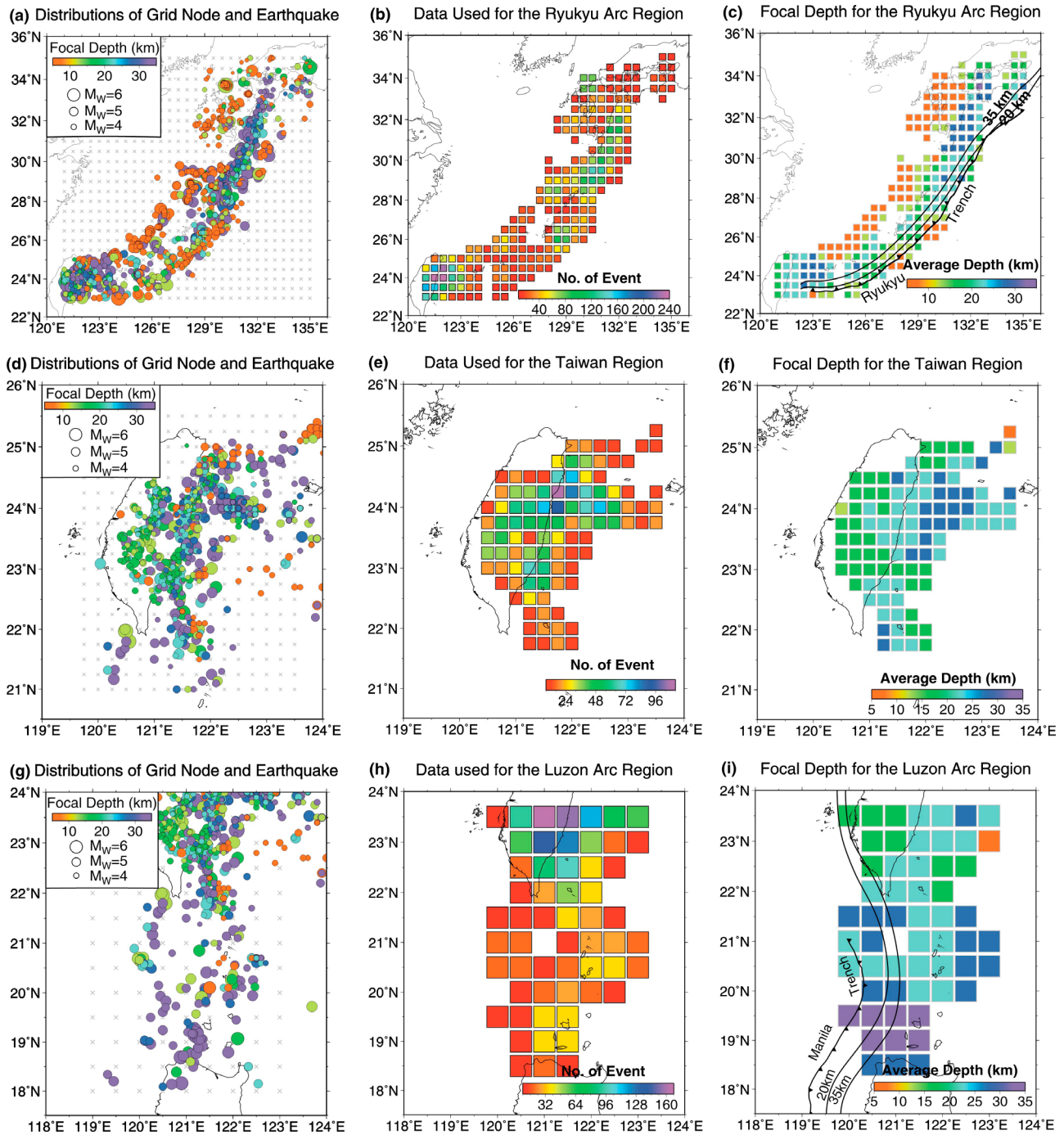


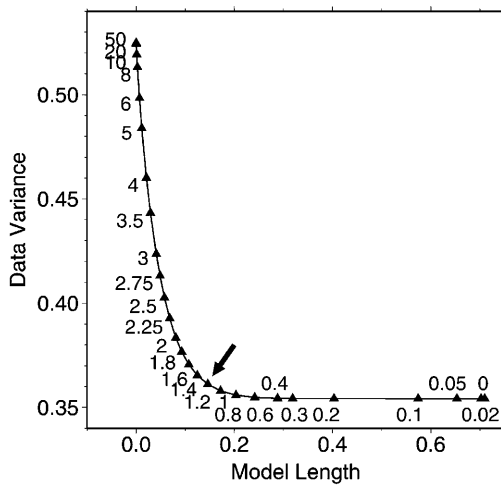
Figure 3. Distributions of the grid nodes (crosses) and earthquakes (circles) used in the stress inversion, the total number of events used in the stress inversion for each node, and the average focal depth of used events for each node and slab geometry of subducted Philippine Sea plate for (a–c) the Ryukyu subduction zone, (d–f) the Taiwan collision zone, and (g–i) the Luzon arc. The grid interval is 0.5° for the Ryukyu and Luzon regions and 0.25° for the Taiwan region. For each grid node, the inversion is skipped if it has less than eight samples.

particular node might be a compromise of two (or even more) neighboring stress regimes, we mark nodes of extreme data diversity (i.e., the averaged angular difference $\geq 85^\circ$) with red inner circles in Figure 5 and dots at the grid centers in Figures 6, 7 and 8. Tectonic interpretation and discussion of these results should be cautious.

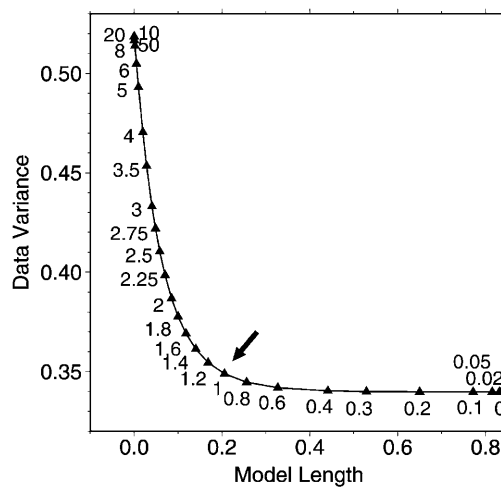
2.3. Checkerboard Tests

[17] To evaluate the capability of the damped stress inversion method in reconstructing the spatial variation of stress direction, we follow the procedure presented by *Hardebeck and Michael* [2006] to perform the checkerboard tests for the three subareas in our study. Based on the

(a) Damping Parameter for the Ryukyu Arc Region



(b) Damping Parameter for the Taiwan Region



(c) Damping Parameter for the Luzon Arc Region

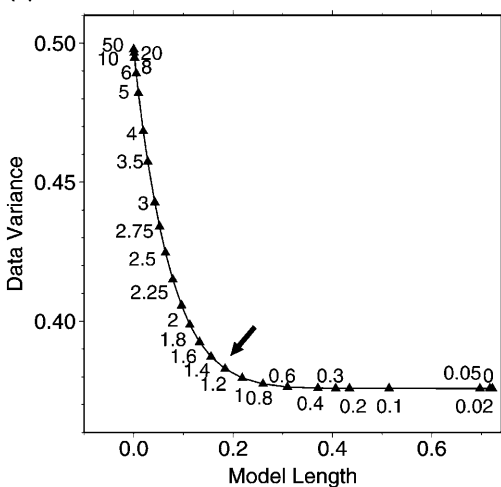


Figure 4. Trade-off curves showing the relation between the model length and data variance for different choices of the damping parameters (triangles). The values used in our final inversion are marked by arrows.

locations and focal mechanisms of our data set, the synthetic checkerboard data are created with alternating states of stress (horizontal σ_1 and σ_3 axes and vertical σ_2 axis, $R = (\sigma_1 - \sigma_2)/(\sigma_1 - \sigma_3) = 0.5$) such that the direction of σ_1 is alternatively assigned to either N-S or N45°E for all grid nodes. Then the rake of each earthquake is set to the direction of the resolved shear stress. We also add random errors (assuming a normal distribution with a standard deviation of 25°) to the strike, dip and rake of the synthetic data to mimic the possible uncertainties in the real data set. The results of our checkerboard tests, presented in Figures S2 and S3 in Text S1, show that most of the inputted checkerboard pattern can be fully recovered by the damped stress inversion method. Most importantly, the true sharp stress variations across the block boundaries are well resolved even with the presence of random errors. Despite the relatively large errors assumed in the synthetic data set (25°), most of the differences between the given and inverted stress directions are less than 15°. These tests successfully demonstrate the robustness of the damped inversion method.

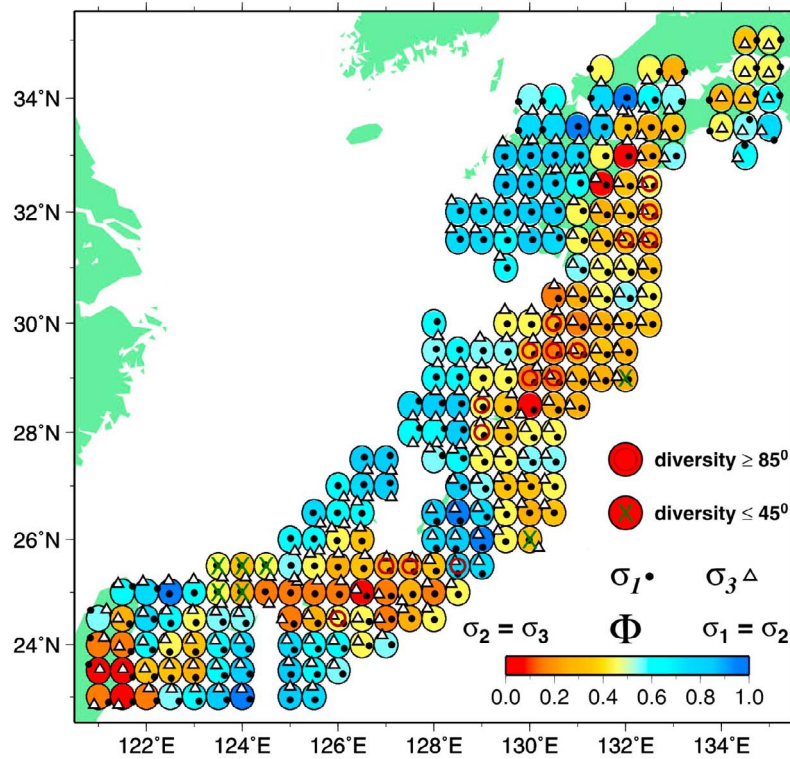
2.4. Sensitivity Tests

[18] Technically, there are three primary factors that might control the stress inversion outcomes: the input data set, the grid size, and the choice of the damping parameter. In practice, the effect of each factor may be intrinsically related to that of another. For example, when the number of available earthquake focal mechanisms is limited, a larger grid size may be required to avoid excessive uncertainty at each grid point. Likewise, a smaller data set may need a slightly larger damping parameter in the inversion to smoothen the overall outcome. Generally speaking, the inversion is considered robust if most of the inverted features remain unchanged with different data sets and/or controlling parameters.

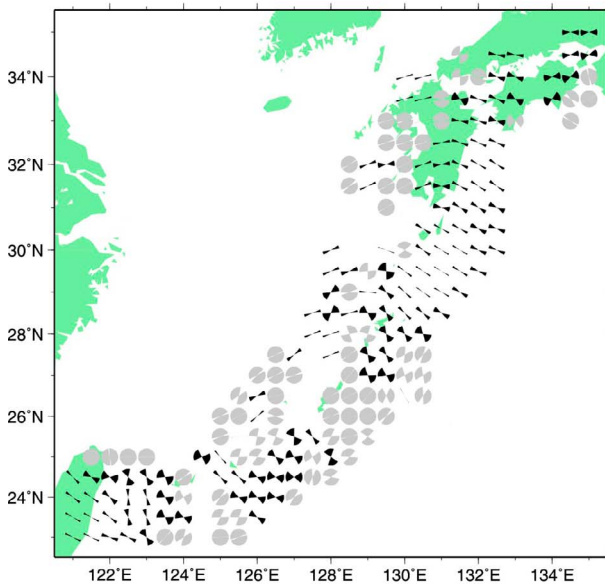
[19] A series of tests have been performed to assess the robustness of our inversion. First, we test if the inversion results might be biased by different data sets. We take the Taiwan region (where the amount of data is most abundant) as an example and repeat the inversion using GCMT catalog only. Although the number of grid nodes with acceptable inversion results becomes smaller, the directions of principal stress axes at nodes within Taiwan and in the immediately offshore area remain the same (the maximum difference is $< 5^\circ$). Similar conclusion can be drawn using a data set without the 1999 Chi-Chi earthquake sequence (main shock $M_w \sim 7.6$ and many aftershocks with $M_w > 6$). For the Ryukyu arc, we also carry out the inversion using earthquakes shallower than 20 km depth to examine the influence of intraplate or interplate earthquakes. It turns out that the directions of principal stress axes at most grid nodes deviate less than 10° from the inversion results using earthquakes down to 35 km depth. This may suggest that our data set is consistent with the assumption of a homogeneous stress regime at each grid point in terms of depth. Few nodes with relatively large difference show odd stress directions, probably related to ill constraints from a small number of focal mechanisms. These tests suggest that a richer data set could sharpen the overall image without introducing unwanted artifacts.

[20] Furthermore, large earthquakes generally bring information about the large-scale stress field only, while small earthquakes can reflect the same overall or locally short-wavelength stress field [Lu et al., 1997]. Therefore if we mix

(a) Inversion Result for the Ryukyu Arc Region



(b) 95% confidence interval for σ_1



(c) 95% confidence interval for σ_3

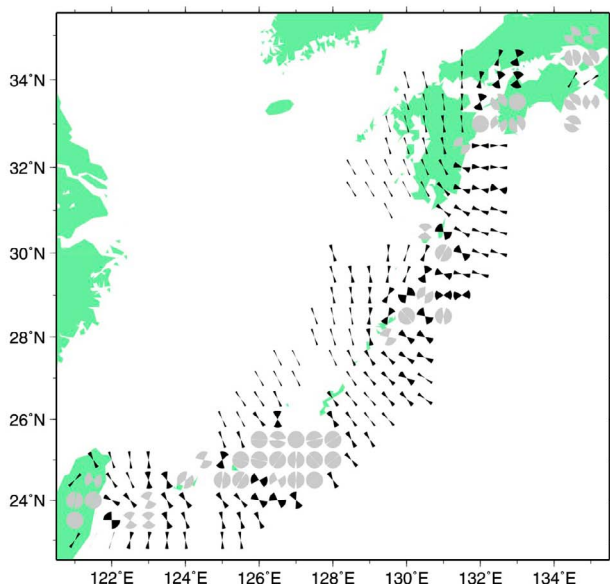
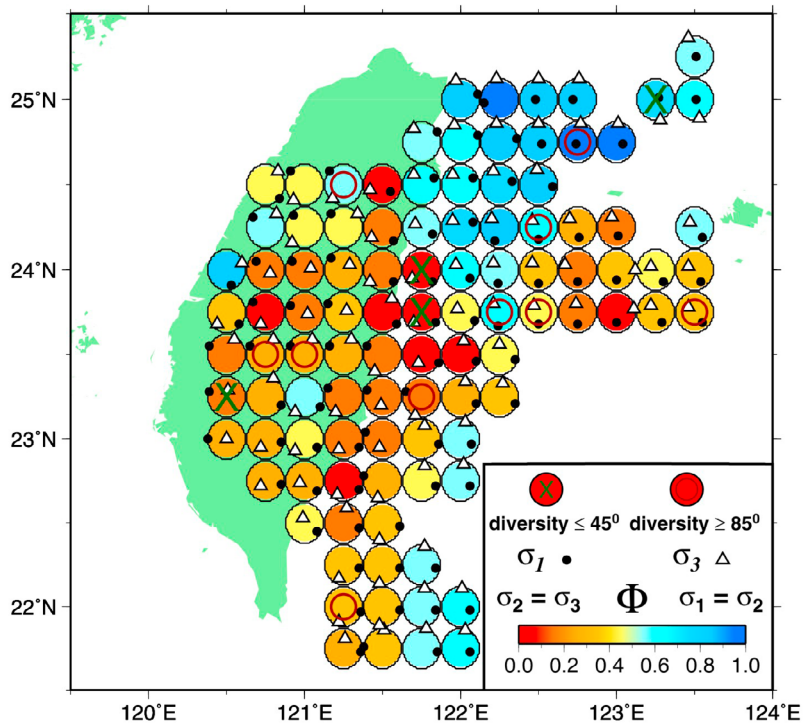
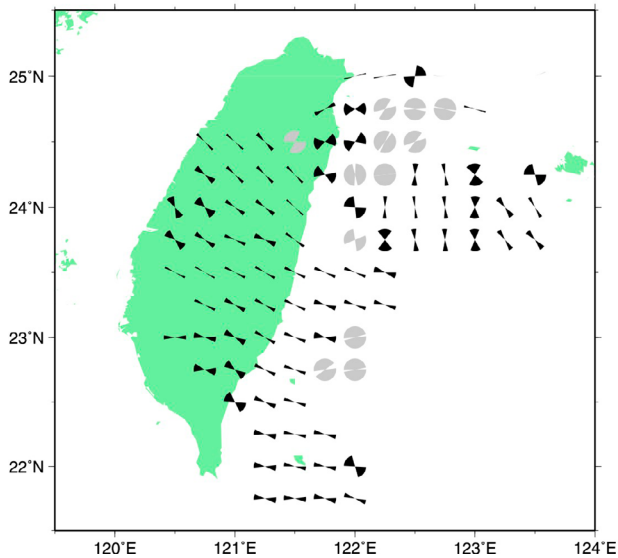


Figure 5. Results of crustal stress inversion for (a–c) the Ryukyu subduction zone, (d–f) the Taiwan collision zone, and (g–i) the Luzon arc. For each grid node, the orientations of σ_1 and σ_3 are marked by lower hemisphere projection with the color showing the corresponding ratio of stress differences, $\Phi = (\sigma_2 - \sigma_3) / (\sigma_1 - \sigma_3)$. A node is marked by a green cross or a red inner circle if the diversity of the focal mechanism data set is $\leq 45^\circ$ or $\geq 85^\circ$, respectively, indicating that the data set either has insufficient constraint on the orientation of the inverted principle stress axes or might be associated with more than one stress regimes. The 95% confidence intervals for the σ_1 and σ_3 directions are estimated by bootstrap resampling of the entire data set for 2000 times and are shown in gray if they are larger than 90° .

(d) Inversion Result for the Taiwan Region



(e) 95% confidence interval for σ_1



(f) 95% confidence interval for σ_3

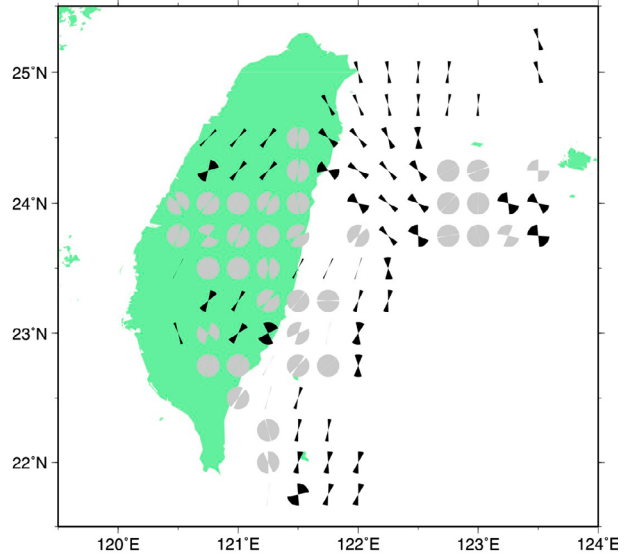


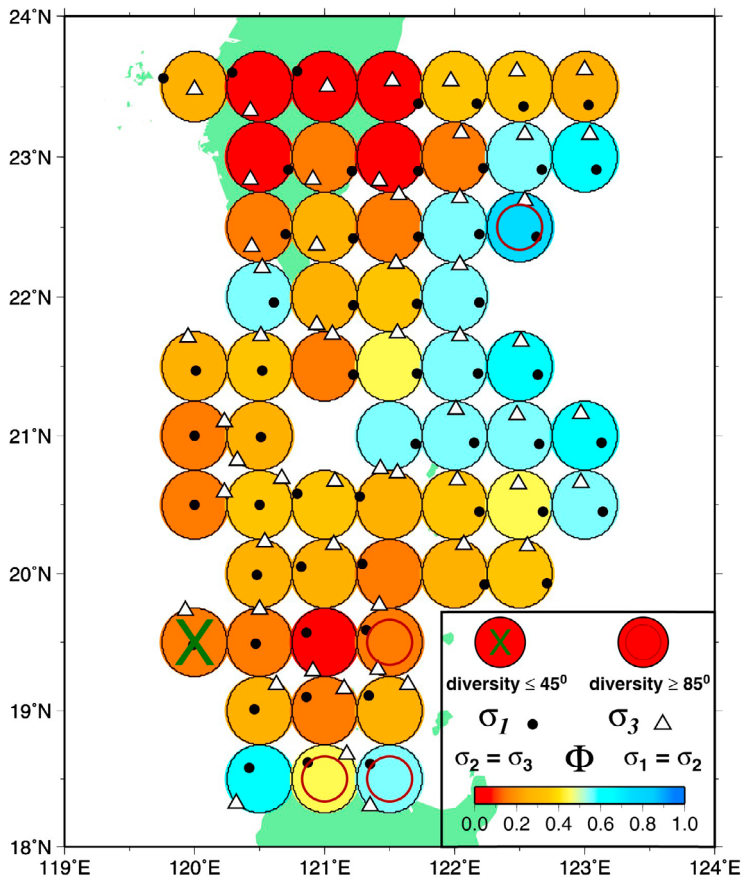
Figure 5. (continued)

the focal mechanisms of both small and large earthquakes to invert stresses, the assumption of stress homogeneity may be invalid. To examine the influence of earthquake rupture dimension, we repeat the stress inversion with two data sets containing large ($M_W \geq 4.5$) and small ($M_W < 4.5$) earthquakes only. When compared with the results derived from the whole data set, the angular differences in the principal stress axes at most grid nodes are minor ($< 10^\circ$). This suggests that, in our

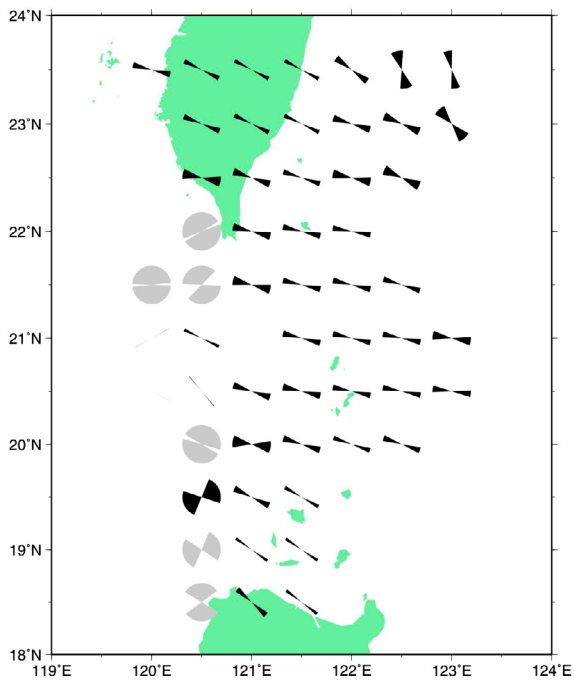
study area, both large and small earthquakes reflect the same regional stress field [e.g., Lu *et al.*, 1997].

[21] Next, we change the grid size of inversion from 0.25° to 0.5° for the Taiwan region. While this experiment has a slightly larger coverage around the edge, its number of grid nodes becomes dramatically smaller. For those nodes solved by both the original inversion (grid size of 0.25°) and this experiment, the vast majority show identical results. A few

(g) Inversion Result for the Luzon Arc Region



(h) 95% confidence interval for σ_1



(i) 95% confidence interval for σ_3

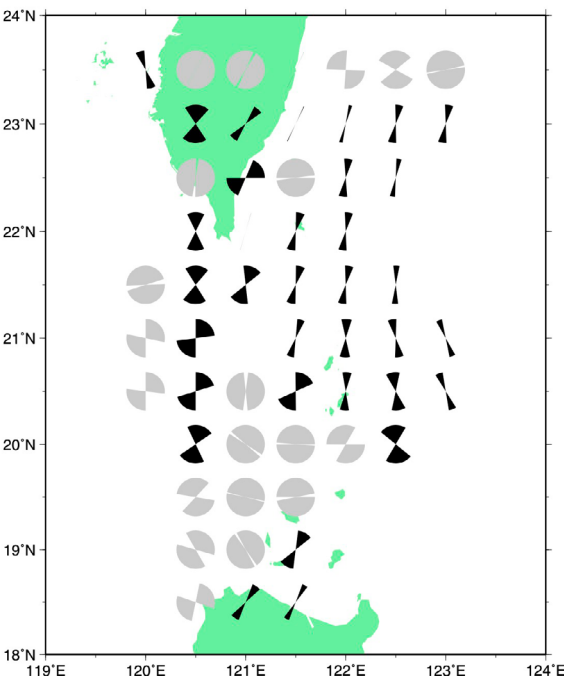
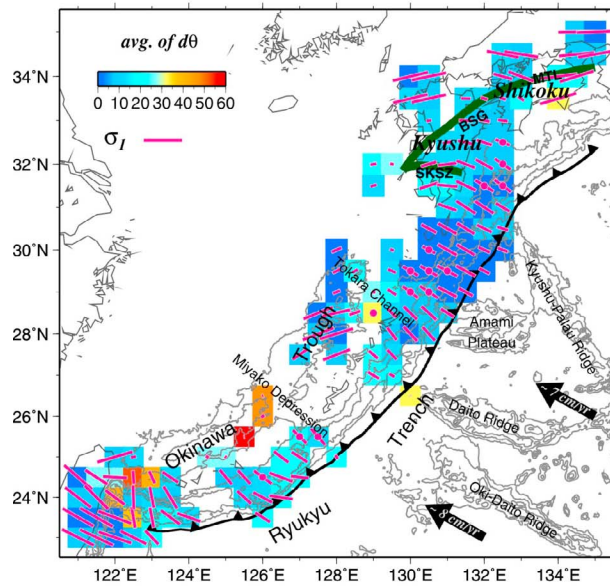
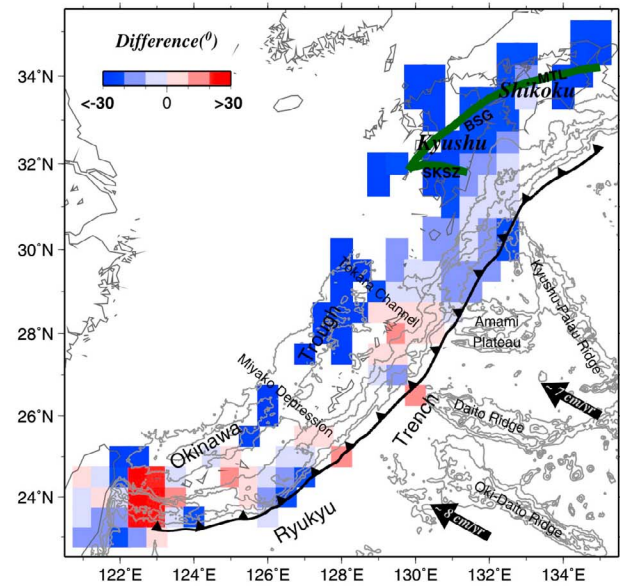


Figure 5. (continued)

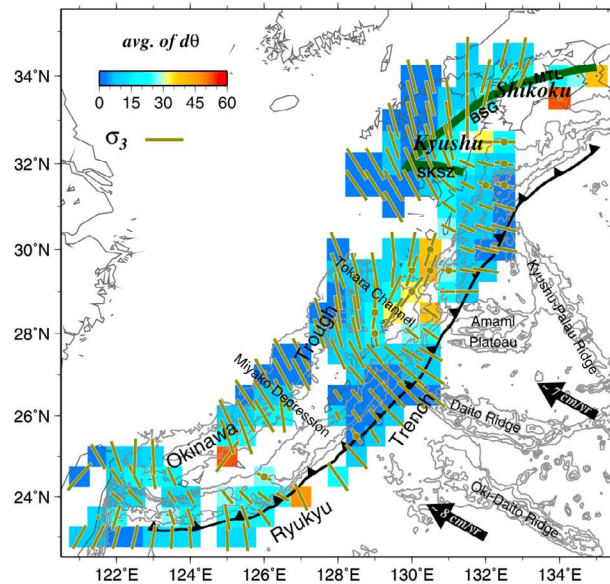
(a) Average Azimuth Difference of σ_1



(b) Direction Difference of σ_1 and Plate Motion



(c) Average Azimuth Difference of σ_3



(d) Tectonic Stress Regime

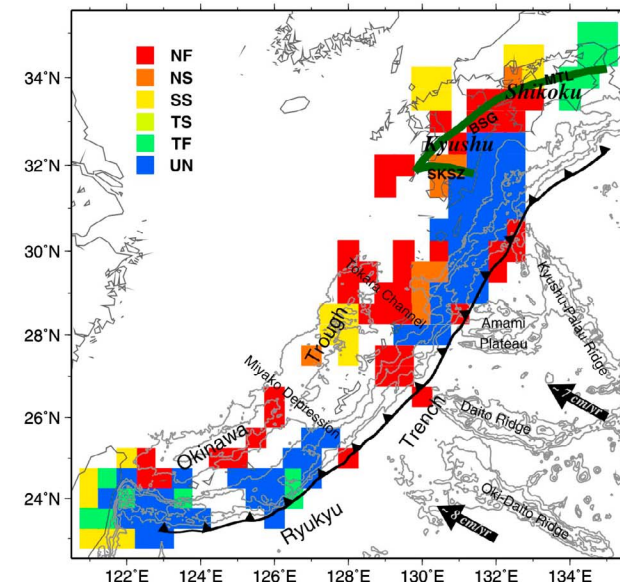
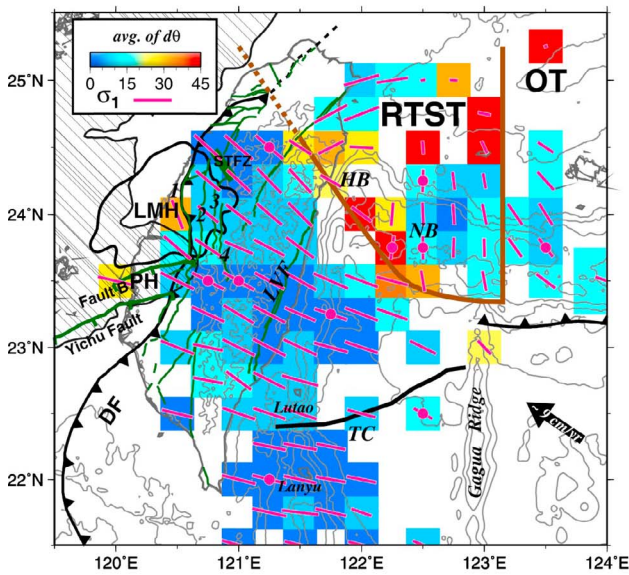
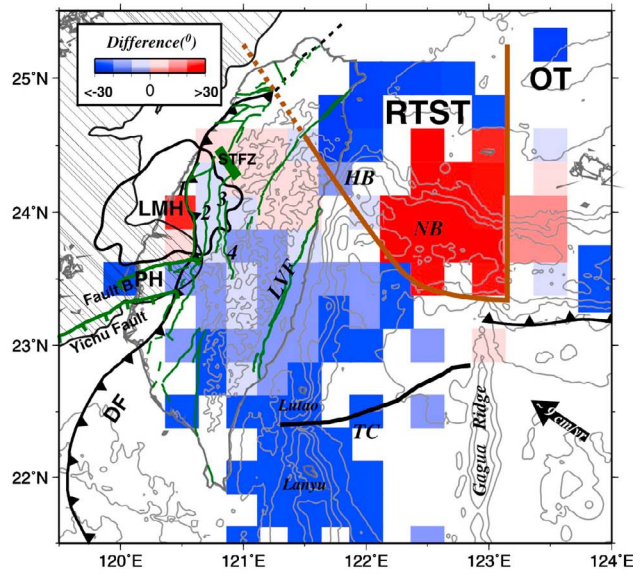


Figure 6. Characteristics of the crustal stress regime in the Ryukyu subduction zone. Bathymetry contour interval is 1000 m. (a) The orientation of σ_1 at each grid node is marked by a pink bar whose length is proportional to the horizontal component. A dot is marked at the center if the data diversity is extreme (Figure 5). The underlying color beneath each node shows the average difference in the σ_1 direction with respect to the neighboring nodes. SKSZ, BSG, and MTL correspond to the South Kyushu Shear Zone, the Beppu-Shimabara Graben, and the Median Tectonic Line, respectively. (b) The azimuthal difference between σ_1 direction and the relative plate motion (N300°) at each node is shown in color. Positive and negative values mean that σ_1 rotates clockwise and counterclockwise with respect to the relative plate motion direction, respectively. (c) Similar to Figure 6a but showing σ_3 in dark green bars. (d) The predominant type of tectonic stress regime at each grid node according to the criteria of Zoback [1992]. NF, normal faulting; NS, predominately normal faulting with a minor strike-slip component; SS, predominately strike-slip faulting with a minor normal or thrust component; TS, predominately thrust faulting with a minor strike-slip component; TF, thrust faulting; UN, unclassified.

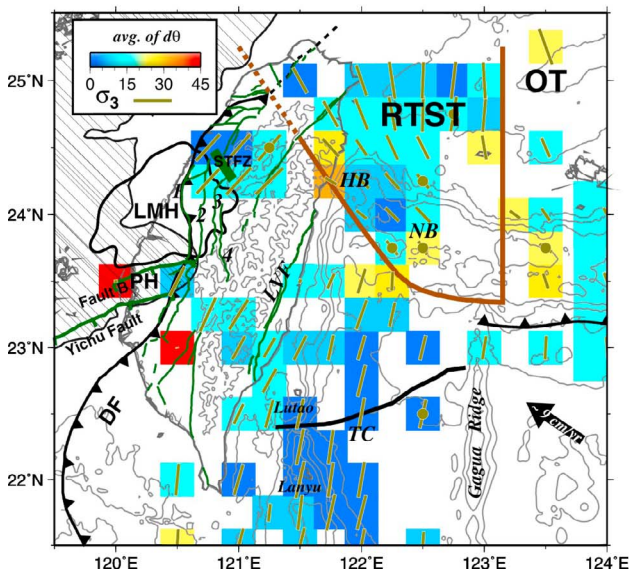
(a) Average Azimuth Difference of σ_1



(b) Direction Difference of σ_1 and Plate Motion



(c) Average Azimuth Difference of σ_3



(d) Tectonic Stress Regime

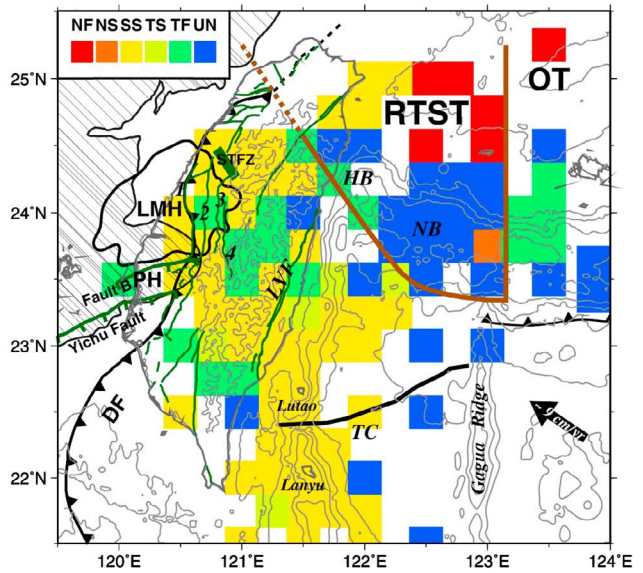


Figure 7. (a–d) Characteristics of the crustal stress regime in the Taiwan collision zone. Layout is the same as that in Figure 6. Boundaries of the Ryukyu-Taiwan Stress Transition (RTST) are marked by brown lines. The Lukang Magnetization High (LMH) is located on the western side of mid-Taiwan, overlapping the northern portion of the Peikang Basement High (PH), as indicated by the 4 km contour of the pre-Miocene basement (hachured area). DF, deformation front; LVF, Longitudinal Valley fault; NB, Nanao Basin; HP, Hoping Basin; TC, Taitung Canyon; STFZ, Sanyi transfer fault zone; 1, Changhua fault; 2, Chelungpu fault; 3, Shantung fault; 4, Shuilikeng fault.

nodes near the edge of the inverted stress regime show slight differences, but none of them is $> 10^\circ$.

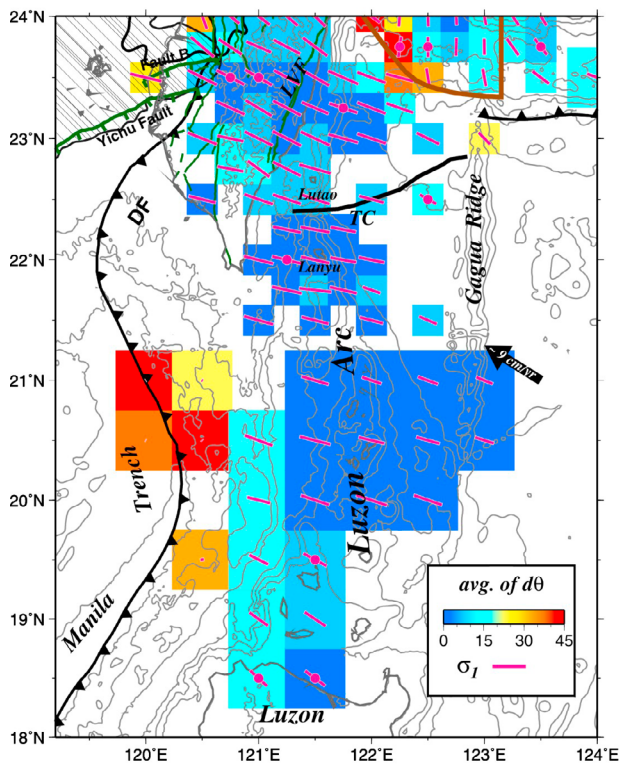
[22] Finally, all inversions are repeated with a wide range of damping parameters (Figure 4) to determine how sensitive the inversion results are to the damping process. As the damping process is critical in minimizing spatial differences across the entire model space, it turns out that the overall

inversion results would not be significantly affected as long as the choice is close (i.e., ± 0.5) to the optimal value.

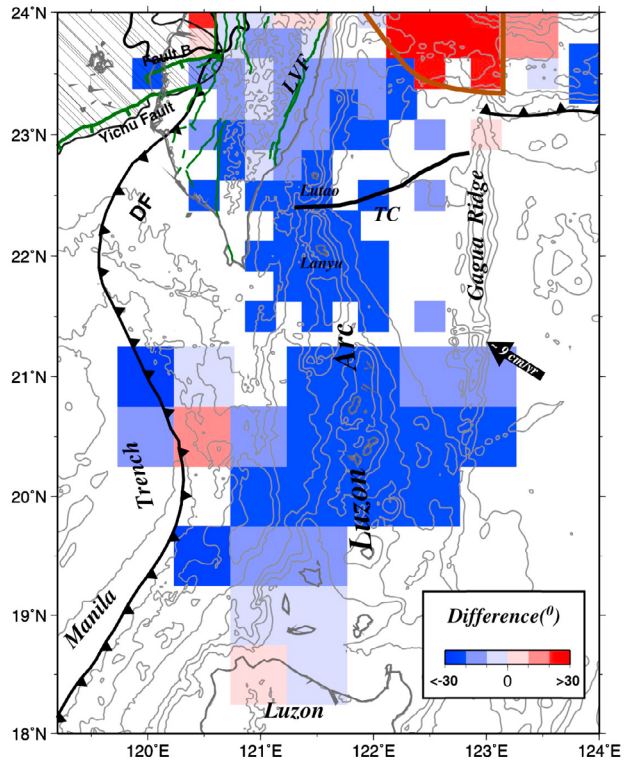
3. Stress Inversion Results and Interpretations

[23] Our inversion results are summarized in Figure 5 (Figures 5a–5c for the Ryukyu arc, Figures 5d–5f for the Taiwan region, and Figures 5g–5i for the Luzon arc). For

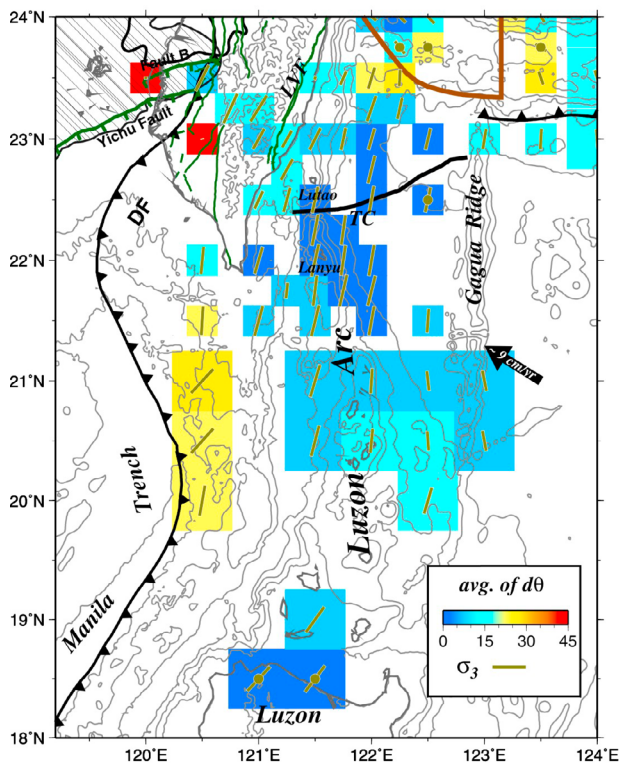
(a) Average Azimuth Difference of σ_1



(b) Direction Difference of σ_1 and Plate Motion



(c) Average Azimuth Difference of σ_3



(d) Tectonic Stress Regime

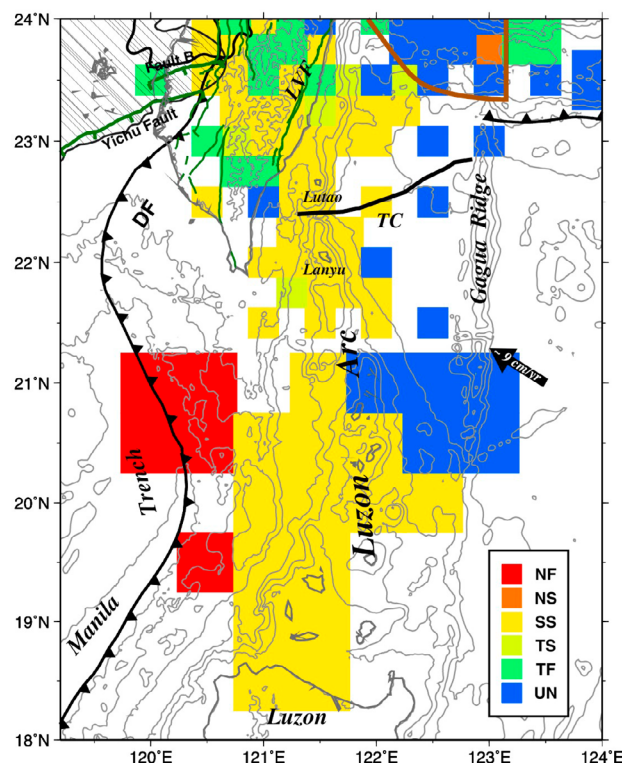


Figure 8. (a–d) Characteristics of the crustal stress regime in the Luzon arc. Layout and symbols are the same as that in Figure 7.

each grid node, the orientations of inverted compressional and extensional stress axes (σ_1 and σ_3) are displayed in lower hemisphere projection with the background color indicating the ratio of stress differences (Φ). The azimuth uncertainties (i.e., 95% confidence interval) of σ_1 and σ_3 vary significantly depending on the corresponding Φ values. In general, very large uncertainties in the azimuths of σ_1 and σ_3 are observed when Φ is close to 1 and 0, respectively. This is primarily due to the likely permutation between two principal stress axes when their difference is small (σ_2 and σ_3 when $\Phi \sim 0$, σ_1 and σ_2 when $\Phi \sim 1$) [e.g., *Hu and Angelier*, 2004]. As a result, we consider the orientation of any stress axis to be tectonically meaningful only if its uncertainty is $< 90^\circ$.

[24] Despite different grid intervals are used in the inversion for different regions, the robustness of our results is well demonstrated by the internal consistency of stress patterns in the overlapping areas of neighboring regions (southwestern Ryukyu arc versus northeast Taiwan, Figure 5a versus Figure 5d; and southeastern Taiwan versus northernmost Luzon arc, Figure 5d versus Figure 5g). To depict the spatial variation quantitatively, we compute the average difference of azimuth ($d\theta$) for σ_1 and σ_3 of each grid node, defines as

$$d\theta = \left(\sum_{i=1}^N |azi_0 - azi_i| \right) / N \quad (1)$$

where azi_0 is the azimuth of the principal stress axis of a given grid node (center), and azi_i is the azimuth of the same principal stress axis at a neighboring node. N is the total number of neighboring nodes (usually is eight, but can be less if the central node is on the model edge). We also calculate the azimuthal difference between each node's σ_1 direction and the predicted relative plate motion to illustrate how σ_1 varies with respect to the plate convergence. Although there are several models for the EP-PSP relative motion [e.g., *Gripp and Gordon*, 2002; *Seno*, 1977; *Seno et al.*, 1993], the estimated directions of relative convergence appear to be very similar. Since we are not concerned with the rate of convergence, we adopt the latest model in this study (i.e., the HS3-NUVEL-1A model [*Gripp and Gordon*, 2002]).

[25] We determine the predominant stress regime at each node following the classification criteria proposed by *Zoback* [1992] (normal faulting, normal faulting with a strike-slip component, strike-slip faulting with a minor normal or thrust component, thrust faulting with a minor strike-slip component, and thrust faulting). When all three axes have intermediate plunges between 25° and 45° or both P and T axes have nearly identical plunges, in the range of 40° and 50° , we assign this kind of stress regime as unknown faulting. For this case, it is difficult to estimate the true maximum and minimum horizontal stress azimuths and may present deformation due to principal stress axes tilted out of horizontal and vertical planes [*Zoback*, 1992]. These results are shown in Figures 6, 7 and 8 for the Ryukyu arc, Taiwan region, and Luzon arc, respectively.

3.1. Stress Field Along the Ryukyu Arc-Trench System

[26] The Ryukyu arc is traditionally divided into three segments (northern, central and southern) by two major left-lateral strike-slip faults of middle Miocene age: the Tokara channel in the north and the Miyako depression in the south

[*Shiono et al.*, 1980; *Kuramoto and Konishi*, 1989] (Figures 1 and 6). The back-arc system to the south of the Tokara channel is currently opening, resulting in a topographic depression known as the Okinawa trough (Figures 1 and 6). Our results indicate that not only the stress regime in the Ryukyu arc-trench region is clearly separated from the Okinawa trough, but also the stress pattern changes significantly from one segment to another (Figure 6). Such a segmented state of stress is in general agreement with previous studies based on the analysis of earthquake source parameters [*Kao and Chen*, 1991; *Kao and Jian*, 2001; *Kao et al.*, 1998b] and numerical modeling [*Hu et al.*, 1996; *Huchon et al.*, 1986], and the details will be discussed in sections 4.1 and 4.2. Along the entire Ryukyu trench and nearby outer rise region, the σ_3 direction is perpendicular to the local strike of the Ryukyu trench (Figure 6c), which is related to the bending of the subducted PSP [*Kao and Chen*, 1991; *Kao et al.*, 1998b].

[27] The stress orientations in Kyushu and southwest Shikoku, Japan, are significantly different from other portions of the Ryukyu subduction zone (Figure 6). Most part of Kyushu is under a normal-faulting stress regime with σ_3 in the NNW-SSE direction (Figures 6c and 6d). This stress field of extension, together with the existence of a clear low P wave velocity zone beneath Kyushu at depths < 40 km [*Wang et al.*, 2008], implies that the opening process of the Okinawa trough may have extended to the northern terminus of the Ryukyu back arc.

[28] The crustal extension beneath Kyushu has a different orientation from the extensional stress field within the subducted PSP slab [*Wang et al.*, 2004], which is dominated by the negative buoyancy with σ_3 in E-W direction. Consequently, we infer that the interplate thrust zone beneath Kyushu is probably decoupled.

[29] Except toward the two ends, the orientations of maximum stress axes (either compression or extension, when they are well constrained; Figures 5a, 5b, and 5c) for most of the Ryukyu fore arc are compatible with the relative plate motion. One special case is found in the arc region near the Tokara channel directly facing the Amami Plateau where the state of stress is characterized by arc-normal compression and arc-parallel extension (Figure 6a and 6c). The σ_1 direction systematically turns counterclockwise with respect to the relative plate motion from the middle segment to the south as the strike of the subduction zone becomes increasingly oblique (Figure 6b).

3.2. Transition From Oblique Subduction to Collision Near the Ryukyu-Taiwan Junction

[30] The southernmost Ryukyu arc-Taiwan region is the most complicated in our study area. The most striking feature in this region is the abrupt change in the σ_1 direction offshore northeast of Taiwan (Figure 7). Specifically, the σ_1 direction agrees with the direction of relative plate motion east of the 123°E meridian but rotates clockwise by $\sim 50^\circ$ to nearly N-S to the west (Figure 7b). It rotates back to the direction of relative plate motion as the Ryukyu trench abuts Taiwan near 121.5°E (Figure 7b). The clockwise and counterclockwise rotations basically mark a triangular area where the tectonic stress regime is unique with respect to the rest of the Ryukyu-Taiwan system. To facilitate our discussion, we refer this triangular area as the Ryukyu-Taiwan Stress Transition (RTST).

[31] The eastern boundary of the RTST, i.e., the 123°E meridian, coincides with the downdip projection of the N–S trending Gagua ridge (Figure 7a and 7b). Because the strike of the Ryukyu subduction zone becomes significantly oblique as it approaches Taiwan, the principal compression can be decomposed into arc-normal (N–S) and arc-parallel (E–W) components. The sudden change of the σ_1 direction from NW–SE to almost N–S along this boundary implies that the arc-parallel component must have been released through internal (aseismic) deformation west of the Gagua ridge. This inference is consistent with the bathymetric evidences of trench-parallel stretching and folding of the Ryukyu fore arc and lateral motions of the Ryukyu accretionary wedge [Dominguez *et al.*, 1998; Lallemand *et al.*, 1999]. Consequently, we conclude that this stress boundary effectively marks the beginning of the transition from Ryukyu subduction to Taiwan collision zones (Figure 7).

[32] On the basis of different data sets, previous studies have proposed a tear fault within the PSP lithosphere to explain the reversal of subduction polarity from Ryukyu (PSP subducting beneath EP) to Luzon (PSP overriding EP) [e.g., Hsu, 2001; Lallemand *et al.*, 1997, 2001]. It is interesting that the surface traces of the proposed tear faults appear to be near the western boundary of the RTST. Although the existence of a lithospheric tear fault remains a subject of controversy [e.g., Chiao *et al.*, 2001; Hsu, 2001; Lallemand *et al.*, 1997, 2001], our results suggest that at least this location is a major stress boundary in regional seismotectonics.

[33] An extensional stress regime is well resolved in the southernmost portion of the Okinawa trough and northeast Taiwan, including the RTST (Figures 5d–5f and 7). However, the σ_3 direction appears to systematically rotate counterclockwise from N–S or NNW–SSE in the east to NW–SE in the west (Figure 7c). Such a pattern presumably is the manifestation of the interaction between the westward expansion of the Okinawa trough rifting and the tectonic collision in central Taiwan [Kao *et al.*, 1998b; Sibuet *et al.*, 1987].

3.3. Stress Variation in the Taiwan Collision Zone

[34] The tectonic stress regime in Taiwan is dominated by compression as the PSP collides with the Eurasia continental margin (Figures 5d–5f and 7). According to paleostress indicators in the Foothill of western Taiwan, Angelier *et al.* [1986] have shown that the compressional stress field exhibits a fan-shaped pattern with the σ_1 direction systematically rotating counterclockwise from north to south. Subsequent studies based on different data sets and/or methodology confirm the existence of σ_1 rotation [e.g., Chang *et al.*, 2003; Hu *et al.*, 1996; Wu *et al.*, 2008; Yeh *et al.*, 1991]. Our results generally agree with such an inference, but indicate that the rotation is not a gradual process throughout Taiwan. Instead, most rotation is observed along localized zones surrounding the mountainous central Taiwan (Figures 5e, 7a and 7b). Specifically, the σ_1 direction maintains within 5° from the relative plate motion for most part of central Taiwan, but deviates by approximately 30° in midwest Taiwan (Figure 7b). These large deviations show clockwise and counterclockwise rotations of the σ_1 axis to the north/northwest and south/southwest, respectively. Notice that the amount of counterclockwise rotation varies significantly from mideast to southeast Taiwan (Figure 7b).

[35] The precise boundary between the clockwise and counterclockwise rotations of the σ_1 axis with respect to the

relative plate motion in western Taiwan coincides with the southern border of a recently discovered magnetic anomaly, named as the Lukang Magnetization High (LMH) (Figure 7b) [Hsu *et al.*, 2008]. Many parameters (e.g., the plate convergent direction, the geometry of the plate boundary, the shape of the collision indenter and rheological properties of major structural units) have been proposed to affect the stress pattern in the Taiwan region [e.g., Hu *et al.*, 1996, 1997]. From our results, the regional stress pattern appears to be closely related to the structural configuration of the LMH, which presumably corresponds to a relatively rigid zone containing mostly igneous rocks [Hsu *et al.*, 2008]. For examples, the eastern front of LMH roughly marks the western end of the predominantly thrust-type regime beneath central Taiwan (Figure 7), whereas the northern limit of the LMH is associated with a strike-slip stress regime (Figure 7d), roughly bounded by the Sanyi-Puli transfer fault zone (a linear NW–SE left-lateral transfer fault system characterized by high electrical conductivity [Chen and Chen, 2002; Deffontaines *et al.*, 1994]). Our observation provides no constraint on the stress regime in the western part of LMH due to the lack of focal mechanism data offshore west of Taiwan (Figures 2, 3d and 3e).

[36] The complex stress pattern surrounding LMH implies that the relatively rigid igneous block may act as a strong indenter for the formation of a foreland fold-and-thrust belt in central west Taiwan involving several major active fault systems (the Sanyi-Puli transfer fault, Suilikeng fault, Shuantung fault, Chelongpu fault, Changhua fault, the Yichu fault, and the Fault B [Lin and Watts, 2002]; Figure 7).

[37] The type of tectonic stress in the central portion of Taiwan is pure thrust (Figure 7d), consistent with the ongoing orogenic process in response to the regional collision. The observed stress regime becomes strike-slip as it moves to both the north and south, facilitating channels of sideway extrusion in northwest and southwest Taiwan [e.g., Kao and Jian, 2001; Shyu *et al.*, 2005].

[38] No change in the σ_1 direction is observed across the Longitudinal Valley fault (LVF) that marks the collision suture between the PSP and EP in eastern Taiwan (Figure 7b). The northernmost end of the Luzon arc abuts Taiwan from southeast (i.e., the Lanyu-Lutao islet chain located offshore southeast of Taiwan; Figure 7). While this region is dominated by tectonic compression induced by the arc-continent collision, the σ_1 axis shows a clear pattern of counterclockwise rotation from north to south (Figure 7b). The deviation of σ_1 direction from the relative plate motion is particularly visible south of the Taitung canyon, a submarine canyon corresponding to a large right-lateral strike-slip fault system [Kao *et al.*, 2000] (Figure 7b). On the basis of bathymetry, seismicity and earthquake source parameters, Kao *et al.* [2000] have demonstrated that the northwestward movement of the PSP could be consumed partly by the deformation across the LVF and the subduction along the Manila trench, and the Taitung canyon fault can accommodate shear component induced in between. Our results confirm that it is also an important structure affecting the regional stress field [W.-N. Wu *et al.*, 2009] (Figure 7).

3.4. Stress Field Along the Manila Trench–Luzon Arc System

[39] The Luzon arc region south of Taitung canyon is dominated by a stress regime of strike-slip type with σ_1 and

σ_3 axes in NW–SEE and NNE–SSW directions, respectively (Figure 8). The overall σ_1 direction appears to deviate from the relative plate motion by approximately 20° counterclockwise for the region north of 19.5°N (Figure 8b). This pattern can be explained by the increasing resistance of the Eurasia continental margin against the indentation of the Luzon arc near Taiwan [e.g., Huang *et al.*, 2000; Kao *et al.*, 2000; Tang and Chemenda, 2000]. Based on the spatial distribution of regional seismicity and characteristics of earthquake source parameters, previous studies have indicated that the region between 21.5°N and 23°N corresponds to a transition from the typical subduction process along the Manila trench to the active collision in Taiwan [e.g., Kao *et al.*, 2000; Tang and Chemenda, 2000]. Our observations suggest that the effect of collision upon the regional tectonic stress field may have reached much farther south to 19.5°N (Figure 8b).

[40] Counterclockwise rotation with respect to the relative plate motion is observed in three (out of a total of four) grid nodes between 18°N and 19°N. The two grid nodes along 18.5°N with extreme data diversity (Figure 5g) suggest that this region may have more than one stress regimes. Nevertheless, the angular differences between σ_1 directions and the relative plate motion are small. Given that the interaction between the EP and PSP becomes increasingly complex south of 19°N [Galgana *et al.*, 2007], additional studies are needed to delineate exactly how the observed σ_1 rotation is related to the local tectonic process.

[41] The tectonic stress near the trench axis and its vicinity is dominated by a complex regime of extension (Figure 8c). The σ_3 direction is consistent with the plate bending along the Manila trench, i.e., perpendicular or subperpendicular to the strike of the trench axis [Kao *et al.*, 2000, 1998b], but quickly rotates to N–S or NE–SW (i.e., parallel or subparallel to the trench axis) as soon as it moves arcward (Figure 8c). This stress pattern is unlikely to be associated with the deformation in the toe of the accretionary prism where trench-normal compression is predominant. It is also difficult to be explained by the lateral membrane stress within the subducted slab accompanying the rapid change of trench geometry from concave to convex, in which case alternative trench-parallel compression and extension regimes are expected [e.g., Chiao, 1993; Strobach, 1973]. In any case, the extensional stress regime is observed only to the south of about 22°N, marking the present-day boundary between the subduction along the Manila trench and the collision in Taiwan (Figure 8).

4. Discussion

[42] Although there is no shortage in the literature focusing on the tectonic stress along the western PSP boundary [e.g., Hsu *et al.*, 2009; Kao and Chen, 1991; Kao and Angelier, 2001; Kao *et al.*, 1998a, 1998b, 2000; Kubo and Fukuyama, 2003; Pezzopane and Wesnousky, 1989; Shiono *et al.*, 1980; Wu *et al.*, 2008; W.-N. Wu *et al.*, 2009], it is rather difficult to directly compare the results of various studies because of the wide differences in the data set and/or processing methodology. A significant advantage of this study is the application of the same inversion scheme to data sets selected with uniform criteria for the entire convergent zone. While our results depict the spatial variation of the

tectonic stress regime of the western PSP boundary in an unprecedented resolution, they can also provide some insight to outstanding issues mentioned in previous studies. In this section, we attempt to revisit some of these important issues.

4.1. Sudden Change in the Crustal Stress Regime Across the Tokara Channel

[43] From focal mechanisms of earthquakes at intermediate depths (>70 km), Kao and Chen [1991] pointed out that the state of stress within the Ryukyu subducted slab is segmented with the north and south under downdip extension and downdip compression, respectively. The switch occurs within a very narrow zone (<100 km) near the Tokara channel (Figure 6). Our results indicate that the Tokara channel also marks an important change in the stress pattern within the crust. Specifically, the number of significant crustal earthquakes in the back-arc region north of the Tokara channel suddenly drops, leaving a significant gap in our data set (Figures 3 and 6). Moreover, the stress regime in the Ryukyu fore arc north of the Tokara channel suddenly has a significant component of arc-parallel extension, and the dimension of this extensional regime approximately coincides with the aseismic region in the back arc (Figure 6c). Because no sudden change in the tectonic parameters (e.g., age and the rate of convergence) is observed across the Tokara channel [e.g., Shiono *et al.*, 1980], the observed sudden variation in the tectonic stress regime is probably related to local features.

[44] One possible factor is the subduction of the Amami plateau whose bathymetric signature is evident to the southeastern side of the Ryukyu trench (Figure 6) [Nakazawa *et al.*, 2008]. Because the Amami plateau has a relatively thicker crust [e.g., Ishihara and Koda, 2007], its subduction might have locally altered the seismogenic conditions in the vicinity of the plate interface and resulted in a chain of active volcanoes in the region (Figure 1). Although exactly how the subducted oceanic plateau may influence the stress regimes in various parts of the subduction system is beyond the scope of this study, our observations suggest that a change in seismogenic behavior as a result of the subduction of a thicker crust could locally modify the directions of principal axes of the corresponding stress regime.

[45] The stress field of arc-parallel extension is localized to the region near the Tokara channel directly facing the Amami plateau (Figure 6c), not throughout the Ryukyu fore arc as reported by Kubo and Fukuyama [2003]. There are at least two factors that may contribute to the inconsistent observations. First, the data set used in the analysis of Kubo and Fukuyama [2003] has significantly less number of events, especially for the southern Ryukyu arc. Second, Kubo and Fukuyama [2003] infer the direction of extensional stress directly from the average direction of the T axes of earthquake focal mechanisms. Such a practice is valid only if earthquakes occur in a homogeneous media without pre-existing weakness [McKenzie, 1969]. Given that Quaternary active faults are observed in the entire Ryukyu arc [e.g., Research Group for Active Faults in Japan, 1991; Ota and Hori, 1980], the formal stress inversion in this study should provide a more realistic picture of the corresponding stress field along the Ryukyu arc.

4.2. Stress Segmentation and Subduction of Seamounts

[46] Although the bathymetric signature of the Okinawa trough is most visible to the south of the Tokara channel (Figures 1 and 6), our results suggest that the entire Ryukyu back arc is characterized by a stress regime of extension (Figure 6d). This observation is consistent with the proposal that the process of back-arc rifting is not limited to the Okinawa trough, but may have extended all the way to the northern terminus near Kyushu [e.g., *Fournier et al.*, 2001; *Sibuet et al.*, 1998].

[47] In general, the observed σ_3 direction is sub-perpendicular to the strike of the arc (Figure 6c). However, a more detailed examination reveals an interesting one-to-one relationship between a change in the orientation of σ_3 and the subduction of a chain of seamounts. From north to south for examples, the subduction of the Kyushu-Palau ridge, the Daito ridge, and the Gagua ridge all correspond to a significant rotation of the extensional axis by as much as 30° (Figures 6b and 7b).

[48] A systematic compilation of active and ancient convergent plate boundaries of the world has led to a conceptual model linking the activation of back-arc rifting/opening, localized rotation of the fore-arc sliver, rapid change in the plate boundary curvature, and the indentation of a buoyant crust [e.g., *Wallace et al.*, 2005, 2009b]. In the case of Ryukyu subduction zone, the collisions with Taiwan in the south and with the Kyushu-Palau ridge in the north have acted as the twin “pinning” points to facilitate the back-arc rifting in the Okinawa trough as a result of the Ryukyu fore-arc rotation (clockwise near the southern end and counterclockwise near the northern) [*McCabe*, 1984; *Letouzey and Kimura*, 1985; *Viallon et al.*, 1986; *Wallace et al.*, 2009a]. Nonetheless, two issues remain unclear: (1) whether or not the kinematic rotation of the fore-arc block is accompanied by a rotation of stress axes in the fore-arc/back-arc region and (2) whether the indentation of the Daito ridge and Gagua ridge into the Ryukyu arc has the same effect as the pinning points on the two ends.

[49] Our results may shed some light on the two questions. To the first-order observation, the apparent coincidence between the stress segmentation in the back arc and the subduction of seamounts suggests that the kinematic arc-fore-arc rotation would have a footprint in the corresponding stress regime. However, the response of the stress system may not be the same as that predicted by the kinematic motion. Taking the Gagua ridge for example, its indentation to the Ryukyu arc would result in a clockwise rotation of the eastside fore arc that may promote the rifting process of the Okinawa trough, according to the conceptual model of *Wallace et al.* [2005]. Our stress inversion shows that the σ_3 direction actually rotates counterclockwise as it moves from west to east across the line (almost N–S to the west and NNW–SSE to the east; Figure 6c). Because the bathymetric signature of the Gagua ridge cannot be clearly identified to the north of 23.5°N , how far has it been subducted beneath the Ryukyu margin is still unclear [*Deschamps et al.*, 1998]. Based on the pattern of cross-back-arc volcanism, *Sibuet et al.* [1998] have suggested that the subducted Gagua ridge can reach as far north as the southern Okinawa trough. In any case, the observed stress pattern near the Gagua ridge is not consistent with the prediction of a kinematic fore-arc

rotation model in response to a subducting seamount. Thus, the stress field in the RTST is more dominated by the combined effects of the arc-continent collision and the back-arc rifting. A quantitative modeling with a realistic configuration of the tectonic components and processes of the region is needed to delineate the complex detail.

[50] It is worth noting that the counterclockwise rotation of the northern Ryukyu arc with respect to Kyushu is visible from GPS measurements and can be associated with a left-lateral shear zone in southern Kyushu near 32°N [*Nishimura and Hashimoto*, 2006]. Whether this shear zone is developed in response to the induced fore-arc rotation as a result of the indentation of the Kyushu-Palau ridge is unclear. Since we do not observe any sudden change in the crustal stress pattern across 32°N (Figure 6a), it is implied that the existence of near-surface structures may have limited effect on the local stress field.

[51] In contrast, there is no indentation of seamounts along the Luzon arc south of Taiwan (Figures 1 and 8). Consequently, the conceptual model of fore-arc rotation in response to the subduction of buoyant indentors cannot be applied. Despite of some subtle variations in the stress pattern as described in the previous text, the Luzon arc appears to be much less segmented than the Ryukyu arc.

4.3. Transition From Subduction to Collision Near Taiwan

[52] The transition from subduction along the Ryukyu arc to collision in Taiwan has been extensively studied with a variety of data sets and methods, including geomorphologic/geophysical observations and numerical/physical modeling [e.g., *Chiao et al.*, 2001; *Chou et al.*, 2006; *Font and Lallemand*, 2009; *Hsu et al.*, 1996; *Hsu*, 2001; *Hu et al.*, 2002; *Kao et al.*, 1998b; *Lallemand et al.*, 1999; *Shyu et al.*, 2005; *F. T. Wu et al.*, 2009]. Our results of crustal stress inversion provide further detail by delineating the triangular RTST with well-defined stress boundaries (Figure 7). This pattern is somewhat different from the gradual shift between the extensional and the compressional stress regimes as suggested by previous studies of numerical modeling [e.g., *Hu et al.*, 2002]. Given the aforementioned fore-arc rotation of the southern Ryukyu as a consequence of the collision in Taiwan, our observation implies that it is relatively easier for the associated deformation to take place along the boundaries of microblocks rather than distribute over a diffuse zone.

[53] On the basis of background seismicity and 3-D velocity structures, *F. T. Wu et al.* [2009] proposed that the surface trace of the PSP’s western boundary (i.e., the Ryukyu trench) extends along the 23.7°N latitude westward to intersect the Longitudinal Valley fault in eastern Taiwan (LVF) (Figure 7). This location is about two grid points south of the stress boundary identified from our observations. It is important to realize that the difference may not necessarily imply a contradiction because the two boundaries are defined by different physics. The stress boundary is intrinsically linked to the dynamic response of the plate system, whereas the boundary proposed by *F. T. Wu et al.* [2009] may represent the rheological difference between the two plates.

[54] Incidentally, the western boundary of RTST is in remarkable agreement with the transition between the stages of postcollision and waning collision in northern Taiwan as outlined by the previous geomorphologic analysis [*Shyu et al.*,

2005]. Therefore from a geodynamic point of view, the region south of RTST, which may be part of EP rheologically [F. T. Wu *et al.*, 2009], is clearly dominated by the compressional stress regime of active collision. This is a critical first-order constraint that must be taken into account for any numerical modeling works in the future.

4.4. Significance of Lukang Magnetization High and Peikang Basement High

[55] The fan-shaped pattern of σ_1 axis in Taiwan was previously modeled by the indentation of PSP onto a pre-Miocene basement high located beneath southwest Taiwan (i.e., the Peikang Basement High (PH); Figure 7) [e.g., Barrier and Angelier, 1986; Hu *et al.*, 1996, 2001; Huchon *et al.*, 1986]. More recent studies also argue that the PH plays a critical role in dictating the regional stress pattern [e.g., Chang *et al.*, 2003; Kao and Angelier, 2001; Lin, 2001; Wu *et al.*, 2008]. For example, Wu *et al.* [2008] proposed that the PH beneath southwest Taiwan could act as a barrier to affect the local stress field based on the correlation between the PH and the distribution of a high- V_p anomaly at the depth range of 17–21 km. A closer examination of the tomographic image indicates that not only the bulk region of the high-velocity anomaly is significantly larger than the PH as defined by the contour of the pre-Miocene basement, but it is also shifted farther to the north where the LMH is located [Wu *et al.*, 2007].

[56] Given that our observations correlate much better with the LMH rather than with the PH, we infer that the LMH is probably a more significant factor in controlling the tectonic stress distribution in the Taiwan region. The resulted compression between the igneous, relatively rigid LMH and the continuously northwestward advance of the PSP is ultimately responsible for the occurrences of large earthquakes in the region such as the 1999 Chi-Chi earthquake sequence. Consequently, we emphasize that the LMH should be properly incorporated in the seismic hazard evaluation for central and western Taiwan.

5. Conclusion

[57] A comprehensive data set of earthquake focal mechanisms consisting solutions from both global and regional CMT catalogs is compiled for the Ryukyu-Taiwan-Luzon convergent margin on the western side of the PSP. By applying a recently developed stress inversion method that simultaneously minimizes the misfit between the stress tensor and focal mechanisms within each subarea and the difference between inverted stress tensors of adjacent subareas, the spatial distribution of tectonic stress in the uppermost 35 km of the lithosphere is shown in an unprecedented resolution.

[58] The overall stress pattern along the Ryukyu subduction zone is segmented with boundaries at or near the places of seamount subduction, including the Tokara channel. This pattern indicates that the kinematic fore-arc rotation would have a footprint in the corresponding stress regime; but the response of the stress system may not be the same as that predicted by the kinematic motion. Furthermore, the effect of kinematic motions along near-surface structures such as the left-lateral shear zone in southern Kyushu near 32°N on the local stress field may be limited. The stress regime beneath Kyushu and southwestern Shikoku is characterized

by NNW–SSE extension, suggesting that the process of the back-arc rifting may have extended to the northern terminus of the Ryukyu back arc.

[59] A triangular area between the southernmost Ryukyu subduction zone and Taiwan is identified with a unique stress regime with σ_1 direction clearly deviated from the relative plate motion, referred as the Ryukyu-Taiwan Stress Transition (RTST). The eastern boundary of the RTST coincides with the downdip projection of the N–S trending Gagua ridge along the 123°E meridian, whereas the western boundary is in good agreement with the border separating the postcollision and waning-collision domains in northern Taiwan.

[60] The deviation of the σ_1 direction from the relative plate motion in the Taiwan collision region is not a gradual, fan-shaped changed as previous studies have suggested. Instead, our results indicate that most stress rotation is observed along localized zones surrounding the mountainous central Taiwan. In fact, variations in the observed stress pattern appear to be closely related to the structural configuration of the LMH, presumably a relatively rigid zone containing mostly igneous rocks located beneath the west part of central Taiwan. The eastern front of LMH roughly marks the western end of the predominantly thrust-type stress regime beneath central Taiwan, whereas the northern and southern sides of the LMH are in strike slip. Since the LMH is probably a more significant factor in controlling the regional stress distribution, we emphasize that LMH should be properly incorporated in the seismic hazard evaluation for central and western Taiwan.

[61] An extensional stress regime is observed along the Manila trench–Luzon arc region, but only to the south of 22°N. This observation implies that 22°N is the northern limit of the contemporary boundary between the subduction along the Manila trench and the collision in Taiwan. Meanwhile, counterclockwise rotation of σ_1 appears to extend to the south along the Luzon arc until ~19.5°N. No significant deviation from the predicted plate convergent direction can be found farther south. We thus infer that the 19.5°N latitude could be the incipient point of the stress regime associated with the Luzon arc–Taiwan collision.

[62] **Acknowledgments.** We thank Jeanne Hardebeck for providing the damped stress inversion code and help on many technical details, Yan Kagan for making the 3-D rotation code available, Andrew Lin for providing the Mesozoic basement contours, Yi-Ching Yeh for preparing magnetization data, and Kyoko Okino for calculating theoretical plate motions. We benefitted from discussion with Po-Fei Chen, Ling-Yun Chiao, Jean-Claude Sibuet, and Kelin Wang. We also thank the Associate Editor and four anonymous reviewers for their helpful comments. Figures were prepared with the Generic Mapping Tool software [Wessel and Smith, 1998]. This manuscript was finished during a visit by one of the authors (W.-N. Wu) to the Pacific Geoscience Centre, Geological Survey of Canada under the financial support of the National Science Council of Taiwan (grant NSC-096-2917-1-008-109). This paper is ESS/GSC contribution 20100012.

References

- Abers, G. A., and J. W. Gephart (2001), Direct inversion of earthquake first motions for both the stress tensor and focal mechanisms and application to southern California, *J. Geophys. Res.*, *106*, 26,523–26,540, doi:10.1029/2001JB000437.
- Angelier, J. (1984), Tectonic analysis of fault slip data sets, *J. Geophys. Res.*, *89*, 5835–5848, doi:10.1029/JB089iB07p05835.
- Angelier, J., E. Barrier, and H.-T. Chu (1986), Plate collision and paleostress trajectories in a fold-thrust belt: The foothills of Taiwan, *Tectonophysics*, *125*, 161–178, doi:10.1016/0040-1951(86)90012-0.

- Arnold, R., and J. Townend (2007), A Bayesian approach to estimating tectonic stress from seismological data, *Geophys. J. Int.*, *170*, 1336–1356, doi:10.1111/j.1365-246X.2007.03485.x.
- Barrier, E., and J. Angelier (1986), Active collision in eastern Taiwan: The coastal range, *Tectonophysics*, *125*, 39–72, doi:10.1016/0040-1951(86)90006-5.
- Bautista, B. C., M. L. P. Bautista, K. Oike, F. T. Wu, and R. S. Punongbayan (2001), A new insight on the geometry of subducting slabs in northern Luzon, Philippines, *Tectonophysics*, *339*, 279–310, doi:10.1016/S0040-1951(01)00120-2.
- Biq, C.-C. (1972), Dual-trench structure in the Taiwan-Luzon region, *Proc. Geol. Soc. China*, *15*, 65–75.
- Chang, C.-P., T.-Y. Chang, J. Angelier, H. Kao, J.-C. Lee, and S.-B. Yu (2003), Strain and stress field in Taiwan oblique convergent system: Constraints from GPS observations and tectonic data, *Earth Planet. Sci. Lett.*, *214*, 115–127, doi:10.1016/S0012-821X(03)00360-1.
- Chen, C., and C. Chen (2002), Sanyi-Puli conductivity anomaly in NW Taiwan and its implication for the tectonics of the 1999 Chi-Chi earthquake, *Geophys. Res. Lett.*, *29*(8), 1166, doi:10.1029/2001GL013890.
- Chiao, L.-Y. (1993), Strain segmentation and lateral membrane deformation rate of the subducted Ryukyu slab, *Isl. Arc*, *2*, 94–103, doi:10.1111/j.1440-1738.1993.tb00077.x.
- Chiao, L.-Y., H. Kao, S. Lallemand, and C.-S. Liu (2001), An alternative interpretation for slip vector residual of subduction interface earthquakes: A case study in the southernmost Ryukyu slab, *Tectonophysics*, *333*, 123–134, doi:10.1016/S0040-1951(00)00271-7.
- Chou, H.-C., B.-Y. Kuo, S.-H. Hung, L.-Y. Chiao, D. Zhao, and Y.-M. Wu (2006), The Taiwan-Ryukyu subduction-collision complex: Folding of a viscoelastic slab and the double seismic zone, *J. Geophys. Res.*, *111*, B04410, doi:10.1029/2005JB003822.
- Christova, C. (2004), Stress field in the Ryukyu-Kyushu Wadati-Benioff zone by inversion of earthquake focal mechanisms, *Tectonophysics*, *384*, 175–189, doi:10.1016/j.tecto.2004.03.010.
- Defontaine, B., J.-C. Lee, J. Angelier, J. Carvalho, and J.-P. Rudant (1994), New geomorphic data on the active Taiwan orogen: A multisource approach, *J. Geophys. Res.*, *99*, 20,243–20,266, doi:10.1029/94JB00733.
- Deschamps, A. E., S. E. Lallemand, and J.-Y. Collot (1998), A detailed study of the Gagua Ridge: A fracture zone uplifted during a plate reorganisation in the Mid-Eocene, *Mar. Geophys. Res.*, *20*, 403–423, doi:10.1023/A:1004650323183.
- Dominguez, S., S. Lallemand, J. Malavieille, and P. Schnürle (1998), Oblique subduction of the Gagua Ridge beneath the Ryukyu accretionary wedge system: Insights from marine observations and sandbox experiments, *Mar. Geophys. Res.*, *20*, 383–402, doi:10.1023/A:1004614506345.
- Dziewonski, A. M., T.-A. Chou, and J. H. Woodhouse (1981), Determination of earthquake source parameters from waveform data for studies of global and regional seismicity, *J. Geophys. Res.*, *86*, 2825–2852, doi:10.1029/JB086iB04p02825.
- Font, Y., and S. Lallemand (2009), Subducting oceanic high causes compressional faulting in southernmost Ryukyu forearc as revealed by hypocentral determinations of earthquakes and reflection/refraction seismic data, *Tectonophysics*, *466*, 255–267, doi:10.1016/j.tecto.2007.11.018.
- Fournier, M., O. Fabbri, J. Angelier, and J.-P. Cadet (2001), Regional seismicity and on-land deformation in the Ryukyu arc: Implications for the kinematics of opening of the Okinawa Trough, *J. Geophys. Res.*, *106*, 13,751–13,768, doi:10.1029/2001JB900010.
- Frohlich, C. (2001), Display and quantitative assessment of distributions of earthquake focal mechanisms, *Geophys. J. Int.*, *144*, 300–308, doi:10.1046/j.1365-246x.2001.00341.x.
- Frohlich, C., and S. D. Davis (1999), How well constrained are well-constrained *T*, *B*, and *P* axes in moment tensor catalogs?, *J. Geophys. Res.*, *104*, 4901–4910, doi:10.1029/1998JB900071.
- Galgana, G., M. Hamburger, R. McCaffrey, E. Corpuz, and Q. Chen (2007), Analysis of crustal deformation in Luzon, Philippines using geodetic observations and earthquake focal mechanisms, *Tectonophysics*, *432*, 63–87, doi:10.1016/j.tecto.2006.12.001.
- Gephart, J. W. (1990), FMSI: A FORTRAN program for inverting fault/slickenside and earthquake focal mechanism data to obtain the regional stress tensor, *Comput. Geosci.*, *16*, 953–989, doi:10.1016/0098-3004(90)90105-3.
- Gephart, J. W., and D. W. Forsyth (1984), An improved method for determining the regional stress tensor using earthquake focal mechanism data: Application to the San Fernando earthquake sequence, *J. Geophys. Res.*, *89*, 9305–9320, doi:10.1029/JB089iB11p09305.
- Gripp, A. E., and R. G. Gordon (2002), Young tracks of hotspots and current plate velocities, *Geophys. J. Int.*, *150*, 321–361, doi:10.1046/j.1365-246X.2002.01627.x.
- Hardebeck, J. L., and E. Hauksson (2001), Crustal stress field in southern California and its implications for fault mechanics, *J. Geophys. Res.*, *106*, 21,859–21,882, doi:10.1029/2001JB000292.
- Hardebeck, J. L., and A. J. Michael (2006), Damped regional-scale stress inversions: Methodology and examples for southern California and the Coalinga aftershock sequence, *J. Geophys. Res.*, *111*, B11310, doi:10.1029/2005JB004144.
- Helffrich, G. R. (1997), How good are routinely determined focal mechanisms? Empirical statistics based on a comparison of Harvard, USGS and ERI moment tensors, *Geophys. J. Int.*, *131*, 741–750, doi:10.1111/j.1365-246X.1997.tb06609.x.
- Hsu, S.-K. (2001), Subduction/collision complexities in the Taiwan-Ryukyu junction area: Tectonics of the northwestern corner of the Philippine Sea plate, *Terr. Atmos. Oceanic Sci.*, *12*, suppl. 5, 209–230.
- Hsu, S.-K., J.-C. Sibuet, S. Monti, C.-T. Shyu, and C.-S. Liu (1996), Transition between the Okinawa trough backarc extension and the Taiwan collision: New insights on the southernmost Ryukyu subduction zone, *Mar. Geophys. Res.*, *18*, 163–187, doi:10.1007/BF00286076.
- Hsu, S.-K., Y.-C. Yeh, C.-L. Lo, A. T. Lin, and W.-B. Doo (2008), Link between crustal magnetization and earthquakes in Taiwan, *Terr. Atmos. Oceanic Sci.*, *19*, 445–450, doi:10.3319/TAO.2008.19.5.445(T).
- Hsu, Y.-J., S.-B. Yu, M. Simons, L.-C. Kuo, and H.-Y. Chen (2009), Interseismic crustal deformation in the Taiwan plate boundary zone revealed by GPS observations, seismicity, and earthquake focal mechanisms, *Tectonophysics*, *479*, 4–18, doi:10.1016/j.tecto.2008.11.016.
- Hu, J.-C., and J. Angelier (2004), Stress permutations: Three-dimensional distinct element analysis accounts for a common phenomenon in brittle tectonics, *J. Geophys. Res.*, *109*, B09403, doi:10.1029/2003JB002616.
- Hu, J.-C., J. Angelier, J.-C. Lee, H.-T. Chu, and D. Byrne (1996), Kinematics of convergence, deformation and stress distribution in the Taiwan collision area: 2-D finite-element numerical modelling, *Tectonophysics*, *255*, 243–268, doi:10.1016/0040-1951(95)00140-9.
- Hu, J.-C., J. Angelier, and S.-B. Yu (1997), An interpretation of the active deformation of southern Taiwan based on numerical simulation and GPS studies, *Tectonophysics*, *274*, 145–169, doi:10.1016/S0040-1951(96)00302-2.
- Hu, J.-C., S.-B. Yu, J. Angelier, and H.-T. Chu (2001), Active deformation of Taiwan from GPS measurements and numerical simulations, *J. Geophys. Res.*, *106*, 2265–2280, doi:10.1029/2000JB900196.
- Hu, J.-C., S.-B. Yu, H.-T. Chu, and J. Angelier (2002), Transition tectonics of northern Taiwan induced by convergence and trench retreat, *Spec. Pap. Geol. Soc. Am.*, *358*, 149–162.
- Huang, C.-Y., P. B. Yuan, C.-W. Lin, T. K. Wang, and C.-P. Chang (2000), Geodynamic processes of Taiwan arc-continent collision and comparison with analogs in Timor, Papua New Guinea, Urals, and Corsica, *Tectonophysics*, *325*, 1–21, doi:10.1016/S0040-1951(00)00128-1.
- Huchon, P., E. Barrier, J.-C. De Bremaecker, and J. Angelier (1986), Collision and stress trajectories in Taiwan: A finite element model, *Tectonophysics*, *125*, 179–191, doi:10.1016/0040-1951(86)90013-2.
- Ishihara, T., and K. Koda (2007), Variation of crustal thickness in the Philippine Sea deduced from three-dimensional gravity modeling, *Isl. Arc*, *16*, 322–337, doi:10.1111/j.1440-1738.2007.00593.x.
- Kagan, Y. Y. (2003), Accuracy of modern global earthquake catalogs, *Phys. Earth Planet. Inter.*, *135*, 173–209, doi:10.1016/S0031-9201(02)00214-5.
- Kagan, Y. Y. (2007), Simplified algorithms for calculating double-couple rotation, *Geophys. J. Int.*, *171*, 411–418, doi:10.1111/j.1365-246X.2007.03538.x.
- Kao, H., and J. Angelier (2001), Stress tensor inversion for the Chi-Chi earthquake sequence and its implications on regional collision, *Bull. Seismol. Soc. Am.*, *91*, 1028–1040, doi:10.1785/0120000739.
- Kao, H., and W.-P. Chen (1991), Earthquakes along the Ryukyu-Kyushu arc: Strain segmentation, lateral compression, and the thermomechanical state of the plate interface, *J. Geophys. Res.*, *96*, 21,443–21,485, doi:10.1029/91JB02164.
- Kao, H., and P.-R. Jian (2001), Seismogenic patterns in the Taiwan region: Insights from source parameter inversion of BATS data, *Tectonophysics*, *333*, 179–198, doi:10.1016/S0040-1951(00)00274-2.
- Kao, H., P. Jian, K. Ma, B. Huang, and C. Liu (1998a), Moment-tensor inversion for offshore earthquakes east of Taiwan and their implications to regional collision, *Geophys. Res. Lett.*, *25*, 3619–3622, doi:10.1029/98GL02803.
- Kao, H., S. J. Shen, and K.-F. Ma (1998b), Transition from oblique subduction to collision: Earthquakes in the southernmost Ryukyu arc-Taiwan region, *J. Geophys. Res.*, *103*, 7211–7229, doi:10.1029/97JB03510.
- Kao, H., G.-C. Huang, and C.-S. Liu (2000), Transition from oblique subduction to collision in the northern Luzon arc-Taiwan region: Constraints from bathymetry and seismic observations, *J. Geophys. Res.*, *105*, 3059–3079, doi:10.1029/1999JB900357.
- Kubo, A., and E. Fukuyama (2003), Stress field along the Ryukyu arc and the Okinawa trough inferred from moment tensors of shallow earthquakes, *Earth Planet. Sci. Lett.*, *210*, 305–316, doi:10.1016/S0012-821X(03)00132-8.

- Kubo, A., E. Fukuyama, H. Kawai, and K. Nonomura (2002), NIED seismic moment tensor catalogue for regional earthquakes around Japan: Quality test and application, *Tectonophysics*, *356*, 23–48, doi:10.1016/S0040-1951(02)00375-X.
- Kuramoto, S., and K. Konishi (1989), The southwest Ryukyu arc is a migrating microplate (forearc sliver), *Tectonophysics*, *163*, 75–91, doi:10.1016/0040-1951(89)90119-4.
- Lallemant, S., C.-S. Liu, and Y. Font (1997), A tear fault boundary between the Taiwan orogen and the Ryukyu subduction zone, *Tectonophysics*, *274*, 171–190, doi:10.1016/S0040-1951(96)00303-4.
- Lallemant, S., C.-S. Liu, S. Dominguez, P. Schnürle, J. Malavieille, and the ACT Scientific Crew (1999), Trench-parallel stretching and folding of forearc basins and lateral migration of the accretionary wedge in the southern Ryukyus: A case of strain partition caused by oblique convergence, *Tectonics*, *18*, 231–247, doi:10.1029/1998TC900011.
- Lallemant, S., Y. Font, H. Bijwaard, and H. Kao (2001), New insights on 3-D plates interaction near Taiwan from tomography and tectonic implications, *Tectonophysics*, *335*, 229–253, doi:10.1016/S0040-1951(01)00071-3.
- Letouzey, J., and M. Kimura (1985), Okinawa Trough genesis: Structure and evolution of the back arc basin development in a continent, *Mar. Pet. Geol.*, *2*, 111–130, doi:10.1016/0264-8172(85)90002-9.
- Lin, A. T., and A. B. Watts (2002), Origin of the West Taiwan basin by orogenic loading and flexure of a rifted continental margin, *J. Geophys. Res.*, *107*(B9), 2185, doi:10.1029/2001JB000669.
- Lin, C.-H. (2001), The 1999 Taiwan earthquake: A proposed stress-focusing, heel shaped model, *Bull. Seismol. Soc. Am.*, *91*, 1053–1061, doi:10.1785/0120000723.
- Lu, Z., M. Wyss, and H. Pulpan (1997), Details of stress directions in the Alaska subduction from fault plane solutions, *J. Geophys. Res.*, *102*, 5385–5402, doi:10.1029/96JB03666.
- McCabe, R. (1984), Implications of paleomagnetic data on the collision related bending of island arcs, *Tectonics*, *3*, 409–428, doi:10.1029/TC003i004p00409.
- McKenzie, D. P. (1969), The relation between fault plane solutions for earthquakes and the directions of the principal stresses, *Bull. Seismol. Soc. Am.*, *59*, 591–601.
- Michael, A. J. (1984), Determination of stress from slip data: Faults and folds, *J. Geophys. Res.*, *89*, 11,517–11,526, doi:10.1029/JB089iB13p11517.
- Michael, A. J. (1987), Use of focal mechanisms to determine stress: A control study, *J. Geophys. Res.*, *92*, 357–368, doi:10.1029/JB092iB01p00357.
- Michael, A. J. (1991), Spatial variations in stress within the 1987 Whittier Narrows, California, aftershock sequence: New techniques and results, *J. Geophys. Res.*, *96*, 6303–6319, doi:10.1029/91JB00195.
- Nakazawa, T., A. Nishimura, Y. Iryu, T. Yamada, H. Shibasaki, and S. Shiokawa (2008), Rapid subsidence of the Kikai seamount inferred from drowned Pleistocene coral limestone: Implication for subduction of the Amami Plateau, northern Philippine Sea, *Mar. Geol.*, *247*, 35–45, doi:10.1016/j.margeo.2007.08.004.
- Nishimura, S., and M. Hashimoto (2006), A model with rigid rotations and slip deficits for the GPS-derived velocity field in southwest Japan, *Tectonophysics*, *421*, 187–207, doi:10.1016/j.tecto.2006.04.017.
- Ota, Y., and N. Hori (1980), Late Quaternary tectonic movement of the Ryukyu islands, Japan (in Japanese), *Quat. Res.*, *18*, 221–240, doi:10.4116/jaqua.18.221.
- Pezzopane, S. K., and S. G. Wesnousky (1989), Large earthquakes and crustal deformation near Taiwan, *J. Geophys. Res.*, *94*, 7250–7264, doi:10.1029/JB094iB06p07250.
- Rau, R.-J., and F. T. Wu (1998), Active tectonics of Taiwan orogeny from focal mechanisms of small-to-moderate-sized earthquakes, *Terr. Atmos. Oceanic Sci.*, *9*, 755–778.
- Rau, R.-J., F. T. Wu, and T.-C. Shin (1996), Regional network focal mechanism determination using 3D velocity model and *SH/P* amplitude ratio, *Bull. Seismol. Soc. Am.*, *86*, 1270–1283.
- Research Group for Active Faults in Japan (1991), *Active Faults in Japan: Sheet Maps and Inventories*, 437 pp., Tokyo Univ. Press, Tokyo.
- Seno, T. (1977), The instantaneous rotation vector of the Philippine Sea plate relative to the Eurasian plate, *Tectonophysics*, *42*, 209–226, doi:10.1016/0040-1951(77)90168-8.
- Seno, T., S. Stein, and A. E. Gripp (1993), A model for the motion of the Philippine Sea plate consistent with NUVEL-1 and geological data, *J. Geophys. Res.*, *98*, 17,941–17,948, doi:10.1029/93JB00782.
- Shiono, K., T. Mikumo, and Y. Ishikawa (1980), Tectonics of the Kyushu-Ryukyu Arc as evidenced from seismicity and focal mechanism of shallow to intermediate-depth earthquakes, *J. Phys. Earth*, *28*, 17–43.
- Shyu, J. B. H., K. Sieh, Y.-G. Chen, and C.-S. Liu (2005), Neotectonic architecture of Taiwan and its implications for future large earthquakes, *J. Geophys. Res.*, *110*, B08402, doi:10.1029/2004JB003251.
- Sibuet, J.-C., et al. (1987), Back arc extension in the Okinawa Trough, *J. Geophys. Res.*, *92*, 14,041–14,063, doi:10.1029/JB092iB13p14041.
- Sibuet, J.-C., B. Deffontaine, S. Hsu, N. Thareau, J. Le Formal, C. Liu, and A. Party (1998), Okinawa trough backarc basin: Early tectonic and magmatic evolution, *J. Geophys. Res.*, *103*, 30,245–30,267, doi:10.1029/98JB01823.
- Strobach, K. (1973), Curvature of island arcs and plate tectonics, *J. Geophys.*, *39*, 819–831.
- Suppe, J. (1984), Kinematics of arc-continent collision, flipping of subduction, and back-arc spreading near Taiwan, *Mem. Geol. Soc. China*, *6*, 21–33.
- Syracuse, E. M., and G. A. Abers (2006), Global compilation of variations in slab depth beneath arc volcanoes and implications, *Geochem. Geophys. Geosyst.*, *7*, Q05017, doi:10.1029/2005GC001045.
- Tang, J.-C., and A. I. Chemenda (2000), Numerical modelling of arc-continent collision: Application to Taiwan, *Tectonophysics*, *325*, 23–42, doi:10.1016/S0040-1951(00)00129-3.
- Terakawa, T., and M. Matsu'ura (2008), CMT data inversion using a Bayesian information criterion to estimate seismogenic stress fields, *Geophys. J. Int.*, *172*, 674–685, doi:10.1111/j.1365-246X.2007.03656.x.
- Tsai, Y.-B., T. Teng, J.-M. Chiu, and H.-L. Liu (1977), Tectonic implications of the seismicity in the Taiwan region, *Mem. Geol. Soc. China*, *2*, 13–41.
- Viallon, C., P. Huchon, and E. Barrier (1986), Opening of the Okinawa basin and collision in Taiwan: A retreating trench model with lateral anchoring, *Earth Planet. Sci. Lett.*, *80*, 145–155, doi:10.1016/0012-821X(86)90028-2.
- Wallace, L. M., M. R. McCaffrey, J. Beavan, and S. Ellis (2005), Rapid microplate rotations and backarc rifting at the transition between collision and subduction, *Geology*, *33*, 857–860, doi:10.1130/G21834.1.
- Wallace, L. M., S. Ellis, K. Miyao, S. Iura, J. Beavan, and J. Goto (2009a), Enigmatic, highly active left-lateral shear zone in southwest Japan explained by aseismic ridge collision, *Geology*, *37*, 143–146, doi:10.1130/G25221A.1.
- Wallace, L. M., S. Ellis, and P. Mann (2009b), Collisional model for rapid fore-arc block rotations, arc curvature, and episodic back-arc rifting in subduction settings, *Geochem. Geophys. Geosyst.*, *10*, Q05001, doi:10.1029/2008GC002220.
- Wang, K., I. Wada, and Y. Ishikawa (2004), Stresses in the subducting slab beneath southwest Japan and relation with plate geometry, tectonic forces, slab dehydration, and damaging earthquakes, *J. Geophys. Res.*, *109*, B08304, doi:10.1029/2003JB002888.
- Wang, Z., R. Huang, J. Huang, and Z. He (2008), P-wave velocity and gradient images beneath the Okinawa Trough, *Tectonophysics*, *455*, 1–13, doi:10.1016/j.tecto.2008.03.004.
- Wessel, P., and W. H. F. Smith (1998), New, improved version of generic mapping tools released, *Eos Trans. AGU*, *79*(47), 579, doi:10.1029/98EO00426.
- Wu, F. T. (1978), Recent tectonics of Taiwan, *J. Phys. Earth*, *26*, suppl., S265–S299.
- Wu, F. T., W.-T. Liang, J.-C. Lee, H. Benz, and A. Villasenor (2009), A model for the termination of the Ryukyu subduction zone against Taiwan: A junction of collision, subduction/separation, and subduction boundaries, *J. Geophys. Res.*, *114*, B07404, doi:10.1029/2008JB005950.
- Wu, W.-N., S.-K. Hsu, C.-L. Lo, H.-W. Chen, and K.-F. Ma (2009), Plate convergence at the westernmost Philippine Sea plate, *Tectonophysics*, *466*, 162–169, doi:10.1016/j.tecto.2007.11.011.
- Wu, Y.-M., C.-H. Chang, L. Zhao, J. B. H. Shyu, Y.-G. Chen, K. Sieh, and J.-P. Avouac (2007), Seismic tomography of Taiwan: Improved constraints from a dense network of strong motion stations, *J. Geophys. Res.*, *112*, B08312, doi:10.1029/2007JB004983.
- Wu, Y.-M., L. Zhao, C.-H. Chang, and Y.-J. Hsu (2008), Focal mechanism determination in Taiwan by genetic algorithm, *Bull. Seismol. Soc. Am.*, *98*, 651–661, doi:10.1785/0120070115.
- Yeh, Y.-H., E. Barrier, C.-H. Lin, and J. Angelier (1991), Stress tensor analysis in the Taiwan area from focal mechanisms of earthquakes, *Tectonophysics*, *200*, 267–280, doi:10.1016/0040-1951(91)90019-0.
- Yin, Z.-M., and G. Ranalli (1993), Determination of tectonic stress field from fault slip data: Toward a probabilistic model, *J. Geophys. Res.*, *98*, 12,165–12,176, doi:10.1029/93JB00194.
- Zoback, M. L. (1992), First- and second-order patterns of stress in the lithosphere: The world stress map project, *J. Geophys. Res.*, *97*, 11,703–11,728, doi:10.1029/92JB00132.

H.-W. Chen and S.-K. Hsu, Institute of Geophysics, National Central University, Chung-Li 32001, Taiwan. (wennan.v.wu@gmail.com)

H. Kao, Geological Survey of Canada, Pacific Geoscience Centre, Sidney, BC V8L 4B2, Canada.

C.-L. Lo and W.-N. Wu, Institute of Earth Sciences, Academia Sinica, 128 Academia Rd., Section 2, Nangang, Taipei 11529, Taiwan.